EPJ manuscript No.
(will be inserted by the editor)

Theoretical study of incoherent ϕ photoproduction on a deuteron target

T. Sekihara[1,2], A. Martínez Torres[2], D. Jido[2], and E. Oset[3]

[1] Department of Physics, Graduate School of Science, Kyoto University, Kyoto, 606-8502, Japan
[2] Yukawa Institute for Theoretical Physics, Kyoto University, Kyoto 606-8502, Japan
[3] Departamento de Física Teórica and IFIC, Centro Mixto Universidad de Valencia-CSIC, Institutos de Investigación de Paterna, Aptdo. 22085, 46071 Valencia, Spain

Received: date / Revised version: date

Abstract. We study the photoproduction of ϕ mesons in deuteron, paying attention to the modification of the cross section from bound protons to the free ones. For this purpose we take into account Fermi motion in single scattering and rescattering of ϕ to account for ϕ absorption on a second nucleon as well as the rescattering of the proton on the neutron. We find that the contribution of the double scattering for ϕ is much smaller than the typical cross section of $\gamma p \to \phi p$ in free space, which implies a very small screening of the ϕ production in deuteron. The contribution from the proton rescattering, on the other hand, is found to be not negligible compared to the cross section of $\gamma p \to \phi p$ in free space, and leads to a moderate reduction of the ϕ photoproduction cross section on a deuteron at forward angles if the LEPS set up is taken into account. The Fermi motion allows contribution of the single scattering in regions forbidden by phase space in the free case. In particular, we find that for momentum transferred squared close to the maximum value, the Fermi motion changes drastically the shape of $d\sigma/dt$, to the point that the ratio of this cross section to the free one becomes very sensitive to the precise value of t chosen, or the size of the bin used in an experimental analysis. Hence, this particular region of t does not seem the most indicated to find effects of a possible ϕ absorption in the deuteron. This reaction is studied theoretically as a function of t and the results are contrasted with recent experiments at LEPS and Jefferson Lab. The effect of the experimental angular cuts at LEPS is also discussed, providing guidelines for future experimental analyses of the reaction.

PACS. 13.60.Le Meson production – 25.20.Lj Photoproduction reactions

1 Introduction

The photoproduction of ϕ mesons on nucleons has attracted much attention, both experimentally [1–6] and theoretically [7–14]. Renewed recent efforts at LEPS [15] have stimulated also theoretical work [16]. The determination of the strangeness content of the nucleon has been one of the motivations for these studies. Tests on Pomeron exchange in this reaction have also been another one of the motivations. Experimental work on the deuteron has been done at LEPS [17] looking for $d\sigma/dt$ close to $t_{\rm max}$ and related theoretical work on near threshold ϕ photoproduction on the deuteron has been done in [18]. Photoproduction of ϕ mesons in nuclei has also been addressed in [19], looking at the transparency ratio [20], deducing from there an enhanced ϕN cross section in nuclei with respect to the one on a free proton. This issue is of relevance to theories on vector modification in a nuclear medium [21, 22]. A theoretical calculation of ϕ photoproduction in nuclei has been performed in [23], and compared with the experimental results of [19]. Very recently there has been further experimental research concerning ϕ production in deuterium. In Ref. [24] ϕ photoproduction near threshold from a deuterium target is studied, concluding that the extracted $d\sigma/dt$ is consistent with predictions based on a quasifree mechanism, in contradiction with the claims done at LEPS in a different momentum transfer region. Our theoretical results support the findings of Ref. [24] and shed light on the different results claimed for the LEPS experiment [17].

In the present work we address the problem of ϕ photoproduction in the smallest nucleus, the deuteron, contrast our finding with those of Ref. [24], and point out missing experimental information for a proper comparison of our results with the recent measurements of Ref. [17]. By analogy to the photoproduction in nuclei we also have here effects of Fermi motion and of ϕ and proton rescatterings, which are studied here in detail and compared to the data. We find small effects of double scattering for ϕ compared to single scattering in consonance with the findings of Ref. [24] except in regions of phase space forbidden to the scattering on free nucleons. The proton rescatter-

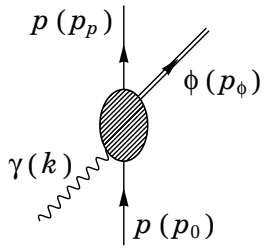

Fig. 1. Kinematics for the $\gamma p \to \phi p$ reaction.

ing effect, on the other hand, is found to be not negligible at the forward angles compared to the single scattering contribution. The Fermi motion effects are also moderate, but of course they are extremely important in the regions forbidden to the scattering on free nucleons. This is the case particularly around the $t_{\rm max}$ region of the free proton, where Fermi motion distorts drastically the shape of the distribution, making this region not well suited to investigate other possible two body mechanisms. The findings of the paper for different values of t and the effect of the angular cuts of the LEPS set up are shown, opening a window for further reanalysis of the reaction of [17] in regions better suited to extract relevant information.

2 Formulation

In this section, we explain our approach to calculate the cross section of the $\gamma p \to \phi p$ and $\gamma d \to \phi p n$ reactions.

2.1 $\gamma p \to \phi p$ reaction

2.1.1 Kinematics

Let us first provide the formulation for the $\gamma p \to \phi p$ reaction. The momenta of the particles in the initial and final states are shown in Fig. 1. In terms of these variables the cross section is defined as,

$$\sigma_{\gamma p\to\phi p}(E_\gamma^{\rm lab}) = \frac{2M_p}{4\sqrt{(k\cdot p_0)^2 - M_\gamma^2 M_p^2}} \int \frac{d^3p_\phi}{(2\pi)^3}\frac{1}{2\omega_\phi}\int \frac{d^3p_p}{(2\pi)^3}\frac{2M_p}{2E_p} \times \overline{\sum_\lambda}\sum_\lambda |T_{\gamma p\to\phi p}|^2 (2\pi)^4\delta^4(k+p_0-p_\phi-p_p), \quad (1)$$

where k, p_0, p_ϕ, and p_p are momenta of initial photon and proton and final ϕ and proton, respectively, and $T_{\gamma p\to\phi p}$ is the scattering amplitude for the $\gamma p \to \phi p$ reaction. By means of the two summation symbols, the sum and average of $|T|^2$ for the polarizations of γ, ϕ, and initial and final protons are done. The cross section is a function of the initial photon energy $E_\gamma^{\rm lab}$ at the laboratory frame where the initial proton is at rest. Using the relation $\sqrt{(k\cdot p_0)^2 - M_\gamma^2 M_p^2} = M_p E_\gamma^{\rm lab}$ and performing the phase-space integration in the center-of-mass frame, one can obtain,

$$\sigma_{\gamma p\to\phi p} = \frac{p'_{\rm cm} M_p}{16\pi^2 E_\gamma^{\rm lab}\sqrt{s}} \int d\Omega_p \overline{\sum_\lambda}\sum_\lambda |T_{\gamma p\to\phi p}|^2, \quad (2)$$

with,

$$p_{\rm cm} = \frac{\lambda^{1/2}(s,\, M_\gamma^2,\, M_p^2)}{2\sqrt{s}}, \quad p'_{\rm cm} = \frac{\lambda^{1/2}(s,\, M_\phi^2,\, M_p^2)}{2\sqrt{s}}, \quad (3)$$

where $p_{\rm cm}$ ($p'_{\rm cm}$) is the initial (final) state momenta in the center-of-mass frame and s the Mandelstam variable $(k+p_0)^2$. In Eq. (2), Ω_p is the solid angle for the final proton in the center-of-mass frame.

For the ϕ photoproduction, the differential cross section $d\sigma/dt$, with Mandelstam variable $t = (p_\phi - k)^2$, is an important observable in the experiments [15,17]. In the center-of-mass frame of the $\gamma p \to \phi p$ reaction, t is written as

$$t = M_\phi^2 - 2p_{\rm cm}(\omega_\phi^{\rm cm} - p'_{\rm cm}\cos\theta_p), \quad (4)$$

with θ_p being the angle between the incident photon and the ϕ meson momenta, and $\omega_\phi^{\rm cm} = \sqrt{M_\phi^2 + p'^2_{\rm cm}}$ the ϕ energy. The maximum and minimum values of t, $t_{\rm max}$ and $t_{\rm min}$, are,

$$t_{\rm max}(s) = M_\phi^2 - 2p_{\rm cm}(\omega_\phi^{\rm cm} - p'_{\rm cm}), \quad (5)$$

$$t_{\rm min}(s) = M_\phi^2 - 2p_{\rm cm}(\omega_\phi^{\rm cm} + p'_{\rm cm}), \quad (6)$$

respectively. Now using the relation,

$$dt = 2p_{\rm cm}p'_{\rm cm} d\cos\theta_p, \quad (7)$$

Eq. (2) can be written as follows:

$$\frac{d\sigma_{\gamma p\to\phi p}}{dt} = \frac{M_p}{16\pi p_{\rm cm} E_\gamma^{\rm lab}\sqrt{s}} \overline{\sum_\lambda}\sum_\lambda |T_{\gamma p\to\phi p}|^2, \quad (8)$$

where we have performed the azimuthal angle integration.

2.1.2 Scattering amplitude

In this section we give details on the scattering amplitude for the $\gamma p \to \phi p$ reaction. In Ref. [15] it was shown that $d\sigma_{\gamma p\to\phi p}/dt$ has an exponential dependence as a function of t. To take this into account we use a phenomenological amplitude given by,

$$T_{\gamma p\to\phi p} = a_p(s)\exp(b\tilde{t}/2) \times \epsilon_\mu(\gamma)\epsilon^\mu(\phi), \quad (9)$$

with $\tilde{t} = t - t_{\rm max}$. Here a_p is a factor which determines the strength of the total cross section. Based on Ref. [25], we take the following s dependence for the factor a_p:

$$a_p(s) = \alpha\left(\frac{s}{\rm GeV^2}\right)^\beta \left[1 + R_a e^{-R_b(E_\gamma^{\rm lab}(s) - R_c)^2}\right]^{1/2}, \quad (10)$$

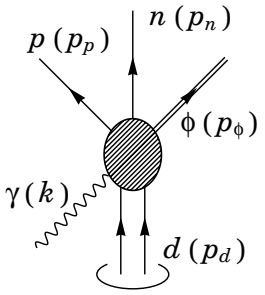

Fig. 2. Kinematics for the $\gamma d \to \phi pn$ reaction.

with parameters $\alpha = 0.0167$ GeV^{-1}, $\beta = 2.29$, $R_a = 0.71$, $R_b = 16.5$ GeV^{-2}, and $R_c = 2$ GeV, so as to reproduce the experimental data [15], and the photon energy $E_\gamma^{\rm lab}$ in a_p is evaluated as $E_\gamma^{\rm lab} = (s - M_p^2)/2M_p$, as a function of s. We note that this form is not same as that in Ref. [25], where the authors fit the differential cross section $d\sigma/dt$ rather than the scattering amplitude. The parameter b in Eq. (9) is taken from [15] as $b = 3.38$ GeV^{-2}. On the other hand, $\epsilon_\mu(\gamma)$ and $\epsilon_\mu(\phi)$ are the photon and ϕ polarization vectors, respectively. In this study we take the Coulomb gauge for the electromagnetic interaction, hence, Eq (9) is rewritten as,

$$T_{\gamma p\to\phi p} = -a_p(s)\exp(b\tilde{t}/2) \times \boldsymbol{\epsilon}(\gamma)\cdot\boldsymbol{\epsilon}(\phi). \tag{11}$$

For the sum over the polarizations, we have the following relations,

$$\sum_{\lambda_\gamma} \epsilon^{*i}(\gamma)\epsilon^{j}(\gamma) = \delta^{ij} - \frac{k^i k^j}{|\boldsymbol{k}|^2}, \tag{12}$$

$$\sum_{\lambda_\phi} \epsilon^{*\mu}(\phi)\epsilon^{\nu}(\phi) = -g^{\mu\nu} + \frac{p_\phi^\mu p_\phi^\nu}{M_\phi^2}. \tag{13}$$

By summing and averaging over the polarizations, we obtain,

$$\overline{\sum_\lambda}\sum_\lambda |T_{\gamma p\to\phi p}|^2 = |a_p|^2\exp(b\tilde{t})\left[1 + \frac{|\boldsymbol{p}_\phi|^2}{2M_\phi^2}\sin^2\theta_p\right], \tag{14}$$

Note that the spin component of the proton does not appear in this phenomenological form of the cross section.

2.2 $\gamma d \to \phi pn$ reaction

2.2.1 Kinematics

Now let us provide the formulation for the $\gamma d \to \phi pn$ reaction. The cross section for the three-body final state is written as [26],

$$\begin{aligned}&\sigma_{\gamma d\to\phi pn}(E_\gamma^{\rm lab}) \\ &= \frac{M_p M_n}{4E_\gamma^{\rm lab}\sqrt{s_{\rm tot}}}\frac{1}{(2\pi)^4}\int dM_{pn}|\boldsymbol{p}_\phi||\boldsymbol{p}_p^*|\int_{-1}^{1} d\cos\theta_\phi \int d\Omega_p^* \\ &\quad\times \overline{\sum_\lambda}\sum_\lambda |T_{\gamma d\to\phi pn}|^2.\end{aligned} \tag{15}$$

Here $s_{\rm tot} = (k + p_d)^2$ is the Mandelstam variable with the initial photon and deuteron momenta, k and p_d, respectively, M_{pn} the p-n invariant mass, $\boldsymbol{p}_\phi$ and θ_ϕ the ϕ momentum and the scattering angle between the incident photon and the final ϕ in the total center-of-mass frame, respectively, and $\boldsymbol{p}_p^*$ and Ω_p^* the proton momentum and the proton solid angle in the p-n center-of-mass frame, respectively.

In order to make connection with the work of [17] we change the integral variables from M_{pn} and $\cos\theta_\phi$ to $t_\phi \equiv (p_\phi - k)^2$ and $u_\phi \equiv (p_\phi - p_d)^2$ with the ϕ momentum p_ϕ. For this purpose we use the following kinematical relations,

$$s_{\rm tot} + t_\phi + u_\phi = M_d^2 + M_\phi^2 + M_{pn}^2, \tag{16}$$

$$s_{\rm tot} - 2\omega_\phi^{\rm cm}\sqrt{s_{\rm tot}} + M_\phi^2 = M_{pn}^2, \tag{17}$$

$$t_\phi = M_\phi^2 - 2E_\gamma^{\rm cm}(\omega_\phi^{\rm cm} - |\boldsymbol{p}_\phi|\cos\theta_\phi), \tag{18}$$

where $E_\gamma^{\rm cm}$ is the photon energy in the total center-of-mass frame, and ϕ energy $\omega_\phi^{\rm cm} = \sqrt{M_\phi^2 + |\boldsymbol{p}_\phi|^2}$. Since $s_{\rm tot}$ is fixed and the masses M_d^2 and M_ϕ^2 are constant, we have from Eq. (16),

$$\frac{\partial M_{pn}}{\partial t_\phi} = \frac{\partial M_{pn}}{\partial u_\phi} = \frac{1}{2M_{pn}}. \tag{19}$$

In addition, since $\omega_\phi^{\rm cm}$ and $|\boldsymbol{p}_\phi|$ are functions of t_ϕ and u_ϕ, we have from Eq. (18),

$$\begin{aligned}\frac{\partial\cos\theta_\phi}{\partial t_\phi} &= \frac{\omega_\phi^{\rm cm}}{4E_\gamma^{\rm cm}\sqrt{s_{\rm tot}}|\boldsymbol{p}_\phi|^3}(t_\phi - M_\phi^2 + 2E_\gamma^{\rm cm}\omega_\phi^{\rm cm}) \\ &\quad + \frac{1}{2E_\gamma^{\rm cm}|\boldsymbol{p}_\phi|}\left(1 - \frac{E_\gamma^{\rm cm}}{\sqrt{s_{\rm tot}}}\right),\end{aligned} \tag{20}$$

$$\begin{aligned}\frac{\partial\cos\theta_\phi}{\partial u_\phi} &= \frac{\omega_\phi^{\rm cm}}{4E_\gamma^{\rm cm}\sqrt{s_{\rm tot}}|\boldsymbol{p}_\phi|^3}(t_\phi - M_\phi^2 + 2E_\gamma^{\rm cm}\omega_\phi^{\rm cm}) \\ &\quad + \frac{1}{2E_\gamma^{\rm cm}|\boldsymbol{p}_\phi|}\left(-\frac{E_\gamma^{\rm cm}}{\sqrt{s_{\rm tot}}}\right).\end{aligned} \tag{21}$$

Here we have used the relation,

$$\frac{\partial|\boldsymbol{p}_\phi|}{\partial t_\phi} = \frac{\partial|\boldsymbol{p}_\phi|}{\partial u_\phi} = \frac{\partial|\boldsymbol{p}_\phi|}{\partial\omega_\phi^{\rm cm}}\frac{\partial\omega_\phi^{\rm cm}}{\partial M_{pn}}\frac{\partial M_{pn}}{\partial t_\phi} = -\frac{\omega_\phi^{\rm cm}}{2\sqrt{s_{\rm tot}}|\boldsymbol{p}_\phi|}, \tag{22}$$

where $\partial\omega_\phi^{\rm cm}/\partial M_{pn} = -M_{pn}/\sqrt{s_{\rm tot}}$ is evaluated from Eq. (17). As a consequence, we have,

$$dM_{pn}d\cos\theta_\phi = J(M_{pn},\cos\theta_\phi;\, t_\phi,\, u_\phi)dt_\phi du_\phi \tag{23}$$

with the Jacobian,

$$J(M_{pn},\cos\theta_\phi;\, t_\phi,\, u_\phi) = \frac{1}{4E_\gamma^{\rm cm}M_{pn}|\boldsymbol{p}_\phi|}. \tag{24}$$

Now we can write down the final form of the total cross section for the $\gamma d \to \phi pn$ reaction as,

$$\sigma_{\gamma d\to\phi pn}(E_\gamma^{\rm lab}) = \frac{M_p M_n}{16(E_\gamma^{\rm lab})^2 M_d}\frac{1}{(2\pi)^4}\int dt_\phi \int du_\phi \frac{|\boldsymbol{p}_p^*|}{M_{pn}} \times \int d\Omega_p^* \overline{\sum_\lambda}\sum_\lambda |T_{\gamma d\to\phi pn}|^2, \quad (25)$$

where we have used $E_\gamma^{\rm cm}\sqrt{s_{\rm tot}} = E_\gamma^{\rm lab} M_d$. Or, equivalently, we have,

$$\frac{d\sigma_{\gamma d\to\phi pn}}{dt_\phi} = \frac{M_p M_n}{16(E_\gamma^{\rm lab})^2 M_d}\frac{1}{(2\pi)^4}\int_{u_{\phi,\rm min}}^{u_{\phi,\rm max}} du_\phi \frac{|\boldsymbol{p}_p^*|}{M_{pn}} \times \int d\Omega_p^* \overline{\sum_\lambda}\sum_\lambda |T_{\gamma d\to\phi pn}|^2, \quad (26)$$

with $u_{\phi,\rm min}$ and $u_{\phi,\rm max}$ the minimum and maximum value of u_ϕ for fixed t_ϕ,

$$u_{\phi,\rm min} = M_\phi^2 + M_d^2 + (M_p+M_n)^2 - s_{\rm tot} - t_\phi, \quad (27)$$
$$u_{\phi,\rm max} = 2M_\phi^2 + M_d^2 - 2\sqrt{s_{\rm tot}}\omega_\phi' - t_\phi, \quad (28)$$

$$\omega_\phi' = \sqrt{p_\phi'^2 + M_\phi^2}, \quad p_\phi' = \frac{M_\phi^2 - t_\phi}{4E_\gamma^{\rm cm}} - \frac{M_\phi^2 E_\gamma^{\rm cm}}{M_\phi^2 - t_\phi}, \quad (29)$$

where $u_{\phi,\rm min}$ ($u_{\phi,\rm max}$) is achieved in the case that M_{pn} has its minimum (maximum) value with fixed t_ϕ (see Eq. (16)). From the kinematics, M_{pn} takes values between,

$$(M_p+M_n)^2 \le M_{pn}^2 \le M_\phi^2 + s_{\rm tot} - 2\sqrt{s_{\rm tot}}\omega_\phi'. \quad (30)$$

We note that both $u_{\phi,\rm min}$ and $u_{\phi,\rm max}$ depend on t_ϕ. We also write down the minimum and maximum t_ϕ of the $\gamma d \to \phi pn$ reaction, $t_{\phi,\rm min}$ and $t_{\phi,\rm max}$, which will be needed for Eq. (25), as,

$$t_{\phi,\rm min} = M_\phi^2 - 2E_\gamma^{\rm cm}(\omega_{\rm max} + p_{\rm max}), \quad (31)$$
$$t_{\phi,\rm max} = M_\phi^2 - 2E_\gamma^{\rm cm}(\omega_{\rm max} - p_{\rm max}), \quad (32)$$

with,

$$\omega_{\rm max} = \sqrt{p_{\rm max}^2 + M_\phi}, \quad (33)$$
$$p_{\rm max} = \frac{\lambda^{1/2}(s_{\rm tot}, M_\phi^2, (M_p+M_n)^2)}{2\sqrt{s_{\rm tot}}}. \quad (34)$$

Here $p_{\rm max}$ corresponds to the maximum momentum for the ϕ in the total center-of-mass frame, in which $M_{pn} = M_p + M_n$.

2.2.2 Scattering amplitude

In this section we develop the formalism to obtain the scattering amplitude for the $\gamma d \to \phi pn$ reaction. Since our aim is to compare our results with [17], where the cross section on the proton of the deuteron is singled out, we also select

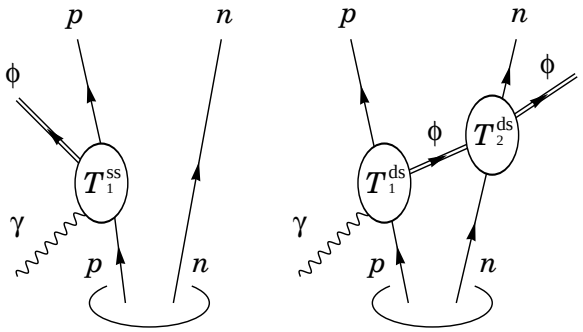

(a) $T^{\rm ss}$ (b) $T^{\rm ds}$

Fig. 3. Diagrams for the calculatin of $\gamma d \to \phi pn$ reaction.

from the full model of the $\gamma d \to \phi pn$ the terms where there is primary production of the ϕ on the proton. It is easy to extend this formulation to a case of the neutron of the deuteron in the same way as the proton case. The ϕ photoproduction amplitude from the proton of the deuteron is obtained from the mechanisms depicted in Fig. 3. The diagram of the left represents the single scattering amplitude, $T^{\rm ss}$. The diagram of the right represents the double scattering amplitude, $T^{\rm ds}$. Modification of the ϕ photoproduction amplitude on the proton of the deuteron with respect to that on a free proton would be attributed to this double scattering amplitude, as well as to Fermi motion and binding effects associated to the deuteron wave function. We will see later that $T^{\rm ss}$ and $T^{\rm ds}$ are correlated destructively with each other. Hence, we expect that $T^{\rm ds}$ decreases the cross section of the impulse approximation.

The evaluation of the amplitude including the deuteron wave function is given in [27], where the authors discussed the $K^- d \to \pi\Sigma n$ reaction. Following [27] we obtain for the impulse approximation amplitude,

$$T^{\rm ss} = T_1^{\rm ss} \times \tilde{\varphi}(|\boldsymbol{p}_n - \boldsymbol{p}_d/2|), \quad (35)$$

written in terms of the elementary $\gamma p \to \phi p$ amplitude $T_1^{\rm ss}$ and the deuteron wave function $\tilde{\varphi}$ in momentum space. The elementary $\gamma p \to \phi p$ amplitude has already appeared in Eq. (11), and we rewrite it for the case of the single scattering in the deuteron target as,

$$T_1^{\rm ss} = -a_p(M_{\phi p}^2)\exp(b\tilde{t}^{\rm ss}/2) \times \boldsymbol{\epsilon}(\gamma)\cdot\boldsymbol{\epsilon}(\phi), \quad (36)$$

where,

$$\tilde{t}^{\rm ss} = (p_\phi - k)^2 - t_{\rm max}(M_{\phi p}^2), \quad (37)$$

with $t_{\rm max}$ defined in Eq. (5). In the case of the single scattering for the $\gamma d \to \phi pn$ reaction, a_p and $t_{\rm max}$ are functions of $M_{\phi p}^2 = (p_\phi + p_p)^2$ instead of s in the free $\gamma p \to \phi p$ reaction.

For the deuteron wave function, we neglect the d-wave component and we use a parameterization of the s-wave component given by an analytic function [28] as,

$$\tilde{\varphi}(p) = \sum_{j=1}^{11}\frac{C_j}{p^2 + m_j^2}, \quad (38)$$

with C_j and m_j determined in [29].

Let us now consider the double scattering amplitude. Following [27], one can show that this amplitude is given by,

$$T^{\rm ds} = \int \frac{d^3q_{\rm ex}}{(2\pi)^3} \frac{\tilde{\varphi}(|\boldsymbol{p}_\phi + \boldsymbol{p}_n - \boldsymbol{q}_{\rm ex} - \boldsymbol{p}_d/2|)}{q_{\rm ex}^2 - M_\phi^2 + iM_\phi\Gamma_\phi} \times T_1^{\rm ds} T_2^{\rm ds}, \tag{39}$$

where $q_{\rm ex}^\mu$ is the exchanged ϕ meson momentum, $T_1^{\rm ds}$ the elementary $\gamma p \to \phi p$ amplitude, and $T_2^{\rm ds}$ the $\phi n \to \phi n$ amplitude. We note that in general both $T_1^{\rm ds}$ and $T_2^{\rm ds}$ depend on $\boldsymbol{q}_{\rm ex}$ and appear inside the $\boldsymbol{q}_{\rm ex}$ integration.

Since we are interested in finding the effects from double scattering, the important point is to pick up the term that leads to largest interference with the impulse approximation, accepting, as it is the case, that the largest contribution is given by the single scattering. For this purpose we take the $\phi n \to \phi n$ amplitude with the same initial and final ϕ polarization. This selects the $\phi n \to \phi n$ amplitude that leads to the same polarization structure as Eq. (36) and hence produces maximum interference with the single scattering amplitude. Explicit details on this $\phi n \to \phi n$ amplitude are given in Appendix A. Then the elementary $\gamma p \to \phi p$ amplitude in Eq. (39) is written as,

$$T_1^{\rm ds} = -a_p((q_{\rm ex} + p_p)^2) \exp(b\tilde{t}'^{\rm ds}/2) \times \boldsymbol{\epsilon}(\gamma) \cdot \boldsymbol{\epsilon}(\phi), \tag{40}$$

with,

$$\tilde{t}'^{\rm ds} = (q_{\rm ex} - k)^2 - t_{\rm max}((q_{\rm ex} + p_p)^2). \tag{41}$$

Hence both the factors a_p and $\exp(b\tilde{t}'^{\rm ds}/2)$ depend on $\boldsymbol{q}_{\rm ex}$. Since the double scattering amplitude is quite small compared to the single scattering one, one can safely approximate $\tilde{t}'^{\rm ds}$ taking into account that the deuteron wave function $\tilde{\varphi}(p)$ takes the largest component when the nucleons are at rest in the rest frame of the deuteron. This allows us to write $(q_{\rm ex} + p_p)^2$ and $(q_{\rm ex} - k)^2$ as,

$$(q_{\rm ex} + p_p)^2 = (k + p_1)^2 \simeq (E_\gamma^{\rm lab} + M_p - B_{1/2})^2 - (E_\gamma^{\rm lab})^2, \tag{42}$$

$$\begin{aligned}(q_{\rm ex} - k)^2 &= (q_{\rm ex}^0 - E_\gamma^{\rm lab})^2 - (\boldsymbol{p}_1 - \boldsymbol{p}_p)^2 \\ &\simeq (q_{\rm ex}^0 - E_\gamma^{\rm lab})^2 - |\boldsymbol{p}_p|^2,\end{aligned} \tag{43}$$

where p_1^μ is the proton momentum inside the deuteron in the laboratory frame, and we take $\boldsymbol{p}_1 \simeq \boldsymbol{0}$ and $p_1^0 = M_p - B_{1/2}$, with $B_{1/2}$ the binding energy for the proton, which we assume to be half of the deuteron binding energy, $B_{1/2} = 1.112$ MeV, and $\boldsymbol{p}_p$ is the final proton momentum in the laboratory frame. Further, $q_{\rm ex}^0$ is approximated in the laboratory frame as,

$$q_{\rm ex}^0 \simeq E_\gamma^{\rm lab} + M_p - B_{1/2} - E_p^{\rm lab}, \tag{44}$$

with $E_p^{\rm lab} = \sqrt{M_p^2 + |\boldsymbol{p}_p|^2}$. Then we have,

$$T_1^{\rm ds} \simeq -a_p(W^2) \exp(b\tilde{t}^{\rm ds}/2) \times \boldsymbol{\epsilon}(\gamma) \cdot \boldsymbol{\epsilon}(\phi), \tag{45}$$

with,

$$\tilde{t}^{\rm ds} = (q_{\rm ex}^0 - E_\gamma^{\rm lab})^2 - |\boldsymbol{p}_p|^2 - t_{\rm max}(W^2), \tag{46}$$

$$W^2 = (E_\gamma^{\rm lab} + M_p - B_{1/2})^2 - (E_\gamma^{\rm lab})^2, \tag{47}$$

with $q_{\rm ex}^0$ given by Eq. (44). Since $T_1^{\rm ds}$ in Eq. (45) no longer depends on $\boldsymbol{q}_{\rm ex}$, we can extract $T_1^{\rm ds}$ outside of the $\boldsymbol{q}_{\rm ex}$ integration in Eq. (39).

Next we consider $T_2^{\rm ds}$, which corresponds to the $\phi n \to \phi n$ amplitude. The details of this amplitude are shown in the Appendix A. As will be clear below, it is through the imaginary part of this amplitude that $T^{\rm ds}$ interferes destructively with the single scattering, once the dominant on-shell part of the intermediate ϕ is taken in $T^{\rm ds}$. In the Appendix A we show that ${\rm Im}T_2^{\rm ds}$ can be approximated by taking $\boldsymbol{q}_{\rm ex} = \boldsymbol{p}_\phi$ if we are concerned about forward ϕ production as one has in the experiment. Yet, since $\tilde{\varphi}(p)$ is very sensitive to the momentum, we do not take $\boldsymbol{q}_{\rm ex} = \boldsymbol{p}_\phi$ in the argument of $\tilde{\varphi}(p)$ in Eq. (39). This approximation allows us to factorize $T_2^{\rm ds}$ outside the integral of Eq. (39), as we had done with $T_1^{\rm ds}$ before.

Now we have only the ϕ meson propagator and the deuteron wave function inside the $\boldsymbol{q}_{\rm ex}$ integral of Eq. (39). For the ϕ meson propagator, we take its imaginary part, keeping the ϕ on-shell, as in Glauber theory, hence,

$$\frac{1}{q_{\rm ex}^2 - M_\phi^2 + iM_\phi\Gamma_\phi} \simeq -i\pi\delta(q_{\rm ex}^2 - M_\phi^2). \tag{48}$$

Using this approximation, one can perform the $\boldsymbol{q}_{\rm ex}$ integration in the laboratory frame as,

$$\begin{aligned}&-i\pi \int \frac{d^3q_{\rm ex}}{(2\pi)^3} \delta(q_{\rm ex}^2 - M_\phi^2) \tilde{\varphi}(|\boldsymbol{p}_\phi + \boldsymbol{p}_n - \boldsymbol{q}_{\rm ex}|) \\ &= \frac{-iq}{8\pi} \int_{-1}^{1} d\cos\theta_q \, \tilde{\varphi}\left(\sqrt{v^2 + q^2 - 2vq\cos\theta_q}\right) \\ &= -i \sum_{j=1}^{11} \frac{C_j}{16\pi v} \ln\left(\frac{(v+q)^2 + m_j^2}{(v-q)^2 + m_j^2}\right),\end{aligned} \tag{49}$$

where $q = \sqrt{q_{\rm ex}^{02} - M_\phi^2}$, $v = |\boldsymbol{p}_\phi + \boldsymbol{p}_n|$, and θ_q is the angle between $\boldsymbol{q}_{\rm ex}$ and $\boldsymbol{p}_\phi + \boldsymbol{p}_n$ in the laboratory frame. To obtain Eq. (49), we have used $\boldsymbol{p}_d = \boldsymbol{0}$ in the laboratory frame and the explicit form of the deuteron wave function of Eq. (38).

As a consequence, we finally have for the double scattering amplitude,

$$T^{\rm ds} = T_1^{\rm ds} \times {\rm Im}\, T_2^{\rm ds}(M_{\phi n}^2) \times \sum_{j=1}^{11} \frac{C_j}{16\pi v} \ln\left(\frac{(v+q)^2 + m_j^2}{(v-q)^2 + m_j^2}\right). \tag{50}$$

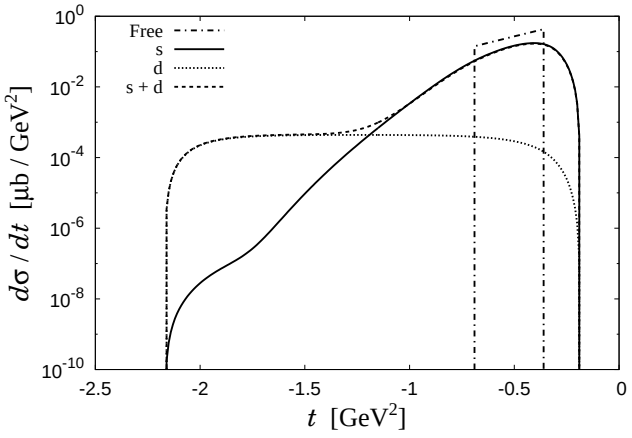

Fig. 4. Differential cross sections $d\sigma_p/dt$ and $d\sigma_{p^*}/dt_\phi$. We fix $E_\gamma^{\rm lab} = 1.6$ GeV. The labels "Free", "s", "d", and "s+d" indicate the case of the free proton target, the single, double, and single plus double scattering case of the deuteron target, respectively.

Then the sum of the amplitudes of the impulse approximation (35) and the double scattering (50) gives us,

$$T^{\rm ss} + T^{\rm ds} = -\boldsymbol{\epsilon}(\gamma)\cdot\boldsymbol{\epsilon}(\phi) \times \Bigg[a_p(M_{\phi p}^2)\exp(b\tilde{t}^{\rm ss}/2)\tilde{\varphi}(|\boldsymbol{p}_n|) + a_p(W^2)\exp(b\tilde{t}^{\rm ds}/2) \times {\rm Im}\, T_2^{\rm ds}(M_{\phi n}^2) \times \sum_{j=1}^{11} \frac{C_j}{16\pi v} \ln\left(\frac{(v+q)^2+m_j^2}{(v-q)^2+m_j^2}\right)\Bigg]. \quad (51)$$

Note that in Eq. (51) we have already made use of the fact that in the Appendix A we chose the part of the $\phi n \to \phi n$ amplitude with the same initial and final ϕ polarizations. It is important to note that the double scattering amplitude $T^{\rm ds}$ is real, like $T^{\rm ss}$, because we have chosen Eq. (48) and Im$T_2^{\rm ds}$. This allows for interference and we find that this interference is destructive, which has the physical meaning that the ϕ produced in the first step of the double scattering can undergo absorption into the $\phi n \to KY$ channels.

3 Results

In this section we will show results for σ_p for the free $\gamma p \to \phi p$ reaction and for the $\gamma d \to \phi pn$, but only for the mechanism where the γ strikes a proton first, as have discussed earlier. We refer to this latter cross section as σ_{p^*}, which one would like to compare with the σ_{p^*} experimental cross section.

3.1 Differential cross sections

First we show in Fig. 4 the differential cross sections $d\sigma_p/dt$ and $d\sigma_{p^*}/dt_\phi$ at $E_\gamma^{\rm lab} = 1.6$ GeV without any angular cuts.

As one can see from Fig. 4, the range of t_ϕ for the deuteron target is wider than for the proton. This is a simple consequence of having a different reaction, $\gamma p \to \phi p$ or $\gamma d \to \phi pn$, where the second one has three particles in the final state and different mass for the target. The limits in either case were given in Eqs. (5) and (6) for the proton and Eqs. (31) and (32) for the deuteron. At $E_\gamma^{\rm lab} = 1.6$ GeV, these values are $t_{\rm min} = -0.69$ GeV^2 and $t_{\rm max} = -0.36$ GeV^2 for the proton and $t_{\phi,{\rm min}} = -2.17$ GeV^2 and $t_{\phi,{\rm max}} = -0.19$ GeV^2 for the deuteron, respectively.

In addition, we should note that at the minimum and maximum values of t for the proton target case the final state phase-space of the reaction $\gamma p \to \phi p$ is finite with a sharp drop to zero, whereas for the deuteron target case the final state phase-space of the reaction $\gamma d \to \phi pn$ goes smoothly to zero. This is a consequence of having three particles in the final state for the deuteron target case. This is shown in Fig. 4 as a smooth decrease of $d\sigma_{p^*}/dt_\phi$ around $t_{\phi,{\rm min}} = -2.17$ GeV^2 and $t_{\phi,{\rm max}} = -0.19$ GeV^2.

For the deuteron target the double scattering amplitude (see Fig. 3(b)), relatively to single scattering, contributes more to $d\sigma_{p^*}/dt_\phi$ in the large $|t_\phi|$ region. This is due to the fact that the large momentum transfer $|t_\phi|$ is achieved only by the large Fermi momentum components in the single scattering. However, in the double scattering this momentum transfer can be split between two nucleons and it is easier to accommodate. Here we also note that the t_ϕ dependence is different for single and double scatterings, and the factor $e^{b\tilde{t}^{\rm ss}}$ strongly suppresses the single scattering contribution in the large t_ϕ region, which is smeared by the split of the momentum transfer in the double scattering. In the small $|t_\phi|$ ($\lesssim 1\,{\rm GeV}^2$) region, on the other hand, the single scattering amplitude dominates $d\sigma_{p^*}/dt_\phi$. Indeed, here one needs only small Fermi momentum components for which the deuteron wave function has its maximum. This result is one of the important findings of the present work. We see that the effect of the double scattering is basically negligible at $t_\phi \simeq t_{\phi,{\rm max}}$ by comparing the curve "s" and "s+d" (where the interference appears). The double scattering alone is less than one per thousand and the interference around $t_{\rm max}$ is less than 7%. The smallness of the double scattering contribution was hinted in Ref. [18] from the fact that the basic experimental information on this reaction was reproduced in terms of single scattering alone. In Ref. [25] the formalism for double scattering was developed for coherent ϕ photoproduction in the deuteron, but no explicit evaluation was done. To the best of our knowledge, this is the first explicit evaluation of the contribution of double scattering for this reaction.

For each photon energy, we show the differential cross sections in Fig. 5, where we plot $d\sigma/dt$ in the $|t| \le 0.8\,{\rm GeV}^2$ region, so as to clarify the behavior of the differential cross sections around the small $|t|$ region. As one can see from the figure, $d\sigma_{p^*}/dt_\phi$ shows the smooth decrease around $t_{\phi,{\rm max}}$, which is not seen in $d\sigma_p/dt$ around $t_{\rm max}$. Also we note that in this t_ϕ region for the $\gamma d \to \phi pn$ reaction the double scattering amplitude interferes destructively with

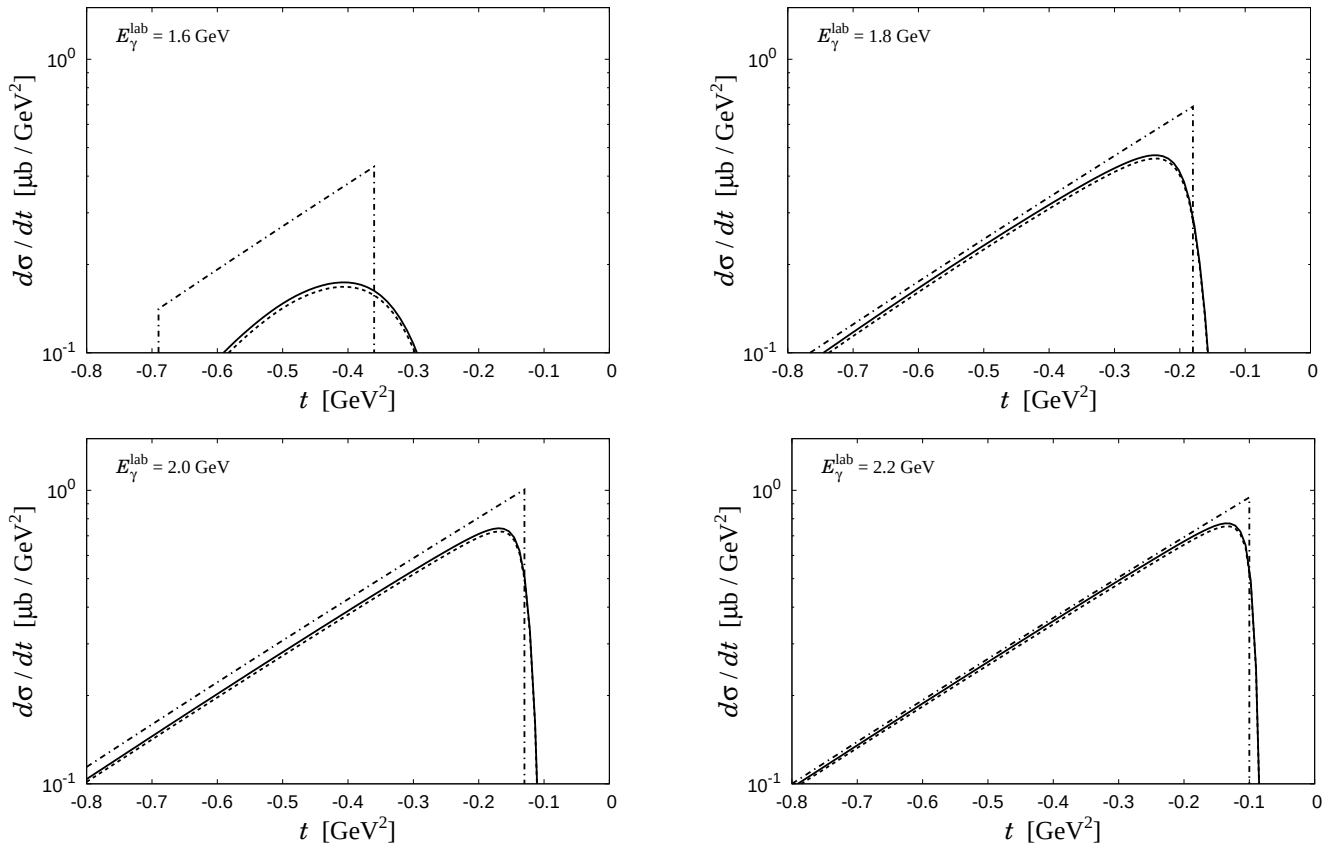

Fig. 5. Differential cross sections $d\sigma_p/dt$ and $d\sigma_{p^*}/dt_\phi$ as functions of t (t_ϕ) for different $E_\gamma^{\rm lab}$. Solid and dashed lines indicate the single and single plus double scattering case of the deuteron target, and dash-doted line the case of the free proton target, respectively.

the single scattering amplitude, although $d\sigma_{p^*}/dt_\phi$ is dominated by the single scattering amplitude.

The results that we find about the accuracy of the single scattering to reproduce the photoproduction cross section in deuteron agree with the conclusions obtained in Ref. [24].

3.2 Nucleon rescattering effects

In the previous subsection we have shown the differential cross sections for the reactions $\gamma p \to \phi p$ and $\gamma d \to \phi pn$. From our results we have found that the "in-medium" ϕ propagation in deuteron, which is realized as a $\phi n \to \phi n$ rescattering in the reaction, has only small contributions to the suppression of the cross section $d\sigma_{p^*}/dt_\phi$ compared to $d\sigma_p/dt$.

Next, let us consider another double-scattering contribution to the cross section $d\sigma_{p^*}/dt_\phi$, that is, the nucleon rescattering effects. In the deuteron target case, this can be taken into account by considering a $pn \to pn$ rescattering as a final state interaction, which is diagrammatically shown in Fig. 6. The scattering amplitude can be evaluated in an analogous way as the ϕ propagation diagrammatically shown in Fig. 3(b), and can be written

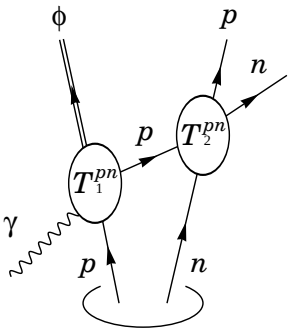

Fig. 6. Diagrams for the nucleon rescattering effects in $\gamma d \to \phi pn$ reaction.

as,

$$T^{pn} = T_1^{pn} \int \frac{d^3q'_{\rm ex}}{(2\pi)^3} \frac{M_p}{E'_{\rm ex}} \frac{\tilde{\varphi}(|\boldsymbol{p}_p + \boldsymbol{p}_n - \boldsymbol{q}'_{\rm ex}|)}{q'^0_{\rm ex} - E'_{\rm ex} + i\epsilon} T_2^{pn}(M_{pn}, \theta_{pn}), \tag{52}$$

where,

$$T_1^{pn} = -a_p(W^2) \exp(b\tilde{t}^{pn}/2) \times \boldsymbol{\epsilon}(\gamma) \cdot \boldsymbol{\epsilon}(\phi), \tag{53}$$

$$\tilde{t}^{pn} = (p_\phi - k)^2 - t_{\rm max}(W^2), \tag{54}$$

$$q'^0_{\rm ex} = E^{\rm lab}_\gamma + M_p - B_{1/2} - \omega^{\rm lab}_\phi, \quad (55)$$

$$E'_{\rm ex} = \sqrt{M_p^2 + |\boldsymbol{q}'_{\rm ex}|^2}, \quad (56)$$

with W^2 defined in Eq. (47) and the ϕ energy in the laboratory frame $\omega^{\rm lab}_\phi$. The $pn \to pn$ scattering amplitude, T_2^{pn}, depends on the p-n invariant mass M_{pn} as well as the scattering angle θ_{pn} in the p-n center-of-mass frame, and will be determined later. For the proton propagator we use an "on-shell" approximation,

$$\frac{M_p}{E'_{\rm ex}} \frac{1}{q'^0_{\rm ex} - E'_{\rm ex} + i\epsilon} \to -2i\pi M_p \delta((q'_{\rm ex})^2 - M_p^2), \quad (57)$$

as for the ϕ propagator in the ϕ exchange amplitude. Then the scattering amplitude can be rewritten as,

$$\begin{aligned} T^{pn} =& \frac{-iM_pT_1^{pn}}{(2\pi)^2} \int_0^\infty d|\boldsymbol{q}'_{\rm ex}||\boldsymbol{q}'_{\rm ex}|^2 \delta(|\boldsymbol{q}'_{\rm ex}|^2 + M_p^2 - (q'^0_{\rm ex})^2) \\ & \times \int d\Omega'_{\rm ex} \tilde{\varphi}(|\boldsymbol{p}_p + \boldsymbol{p}_n - \boldsymbol{q}'_{\rm ex}|) T_2^{pn}(M_{pn}, \theta_{pn}) \\ =& \frac{-iM_pT_1^{pn}}{8\pi^2} \sqrt{q'^0_{\rm ex} - M_p^2} \int d\Omega'_{\rm ex} \tilde{\varphi}(|\boldsymbol{p}_p + \boldsymbol{p}_n - \boldsymbol{q}'_{\rm ex}|) \\ & \times T_2^{pn}(M_{pn}, \theta_{pn}). \end{aligned} \quad (58)$$

Here we emphasize that the solid angle $\Omega_{\rm ex}$ and the momenta $\boldsymbol{p}_p$, $\boldsymbol{p}_n$, and $\boldsymbol{q}'_{\rm ex}$ are evaluated in the laboratory frame, whereas θ_{pn} is evaluated in the p-n center-of-mass frame as $\cos\theta_{pn} = (\boldsymbol{q}'_{\rm ex} \cdot \boldsymbol{p}_p)_{pn}/(|\boldsymbol{q}'_{\rm ex}||\boldsymbol{p}_p|)_{pn}$.

For the determination of the $pn \to pn$ scattering amplitude, we take the following procedure. First, in order to take into account the angular dependence we parameterize the $pn \to pn$ differential cross section as follows:

$$\frac{d\sigma_{pn\to pn}}{d\Omega_{pn}}(M_{pn}, \theta_{pn}) = \mathcal{A}(M_{pn}) + \mathcal{B}(M_{pn}) \cos^2\theta_{pn}. \quad (59)$$

Here spin average and sum are assumed to be taken in the initial and final states, respectively. The parameters $\mathcal{A}$ and $\mathcal{B}$ are determined so as to reproduce the differential cross section. In this study we use experimental data for the total cross section from [26] and model calculation for the differential cross section at $\theta_{pn} = 90$ degrees from [30]. Next we evaluate the real part of the $pn \to pn$ scattering amplitude by assuming that the magnitude of the real part is larger than that of the imaginary part and that the real part dominates the cross section, which is certainly the case at low energies, of relevance to the present problem, where $\mathrm{Im}\, T_2^{pn}$ goes to zero:

$$\mathrm{Re}\, T_2^{pn}(M_{pn}, \theta_{pn}) = \sqrt{\mathcal{A} + \mathcal{B}\cos^2\theta_{pn}} \frac{2\pi M_{pn}}{M_p M_n}. \quad (60)$$

The imaginary part of the $pn \to pn$ amplitude, on the other hand, is evaluated so as to satisfy the optical theorem and to have the same angular dependence as the real part as,

$$\begin{aligned} & \mathrm{Im}\, T_2^{pn}(M_{pn}^2, \theta_{pn}) \\ & = -\sqrt{\frac{\mathcal{A} + \mathcal{B}\cos^2\theta_{pn}}{\mathcal{A} + \mathcal{B}}} \frac{p^{pn}_{\rm cm} M_{pn}}{2M_pM_n} \sigma_{pn\to X}(M_{pn}), \end{aligned} \quad (61)$$

where $p^{pn}_{\rm cm}$ is the center-of-mass momentum of the p-n system and the $pn \to X$ total cross section $\sigma_{pn\to X}$ is obtained by fitting the experimental data given in [26].

Now let us see how the whole $\gamma d \to \phi pn$ reaction is affected by the $pn \to pn$ rescattering effect, for which the amplitude can be expressed as,

$$\begin{aligned} T^{pn} =& \frac{M_pT_1^{pn}}{8\pi^2} \sqrt{q'^0_{\rm ex} - M_p^2} \int d\Omega'_{\rm ex} \tilde{\varphi}(|\boldsymbol{p}_p + \boldsymbol{p}_n - \boldsymbol{q}'_{\rm ex}|) \\ & \times [\mathrm{Im}\, T_2^{pn}(M_{pn}, \theta_{pn}) - i\mathrm{Re}\, T_2^{pn}(M_{pn}, \theta_{pn})]. \end{aligned} \quad (62)$$

First, we note that the first scattering amplitude, T_1^{pn}, shows the same $t_\phi = (p_\phi - k)^2$ dependence as the impulse approximation, $T^{\rm ss}$. This indicates that, in contrast to the ϕ rescattering, the pn rescattering effect has a possibility to become large in the small $|t_\phi|$ region. Next, the imaginary part of the $pn \to pn$ amplitude, $\mathrm{Im}\, T_2^{pn}$, interferes destructively with the single scattering contribution, as one can see from comparing Eqs. (51) and (62) (note that $\mathrm{Im}\, T_2^{pn} \le 0$ due to the optical theorem). This means that in the reaction $\gamma d \to \phi pn$ the final-state proton and neutron are distorted by the pn rescattering, changing directions of the final proton and neutron with regard to single scattering. However, the cross section for the $\gamma d \to \phi pn$ should not be changed by the inclusion of the pn rescattering if one observes the final-state proton and neutron in the whole solid angle (or equivalently one does not observe the proton and neutron), since the proton and neutron cannot disappear in the rescattering process, in contrast to the $\phi n \to \phi n$ rescattering where only the large ϕ absorption part of the amplitude was considered (see Appendix). The recovery of the cross section after the $pn \to pn$ rescattering is realized by the term containing the real part of the pn amplitude, $\mathrm{Re}\, T_2^{pn}$, which is the sole pure imaginary term in Eq. (62) and is added incoherently to the $\gamma d \to \phi pn$ cross section, compensating the destructive interference of the term containing $\mathrm{Im}\, T_2^{pn}$.

The numerical results of $\gamma d \to \phi pn$ cross section with the coherent sum of the three amplitudes (one single and two double scatterings, ϕ and proton exchanges), are shown in Fig. 7 by the dashed line. The contribution only from the proton rescattering is also plotted as the dotted line. As one can see from Fig. 7, the values of the cross section are almost unchanged by the inclusion of the proton rescattering effect. This takes place due to, as explained before, the competition between the imaginary part of the $pn \to pn$ amplitude, which produces destructive interference with the single scattering, and the real part of the $pn \to pn$ amplitude, which contributes incoherently to the cross section.

However, the contribution from the proton rescattering itself is not negligible compared to the cross section only with the single scattering, as seen by the dotted line in Fig. 7. It is important to note that the contribution from the proton rescattering gets large as t_ϕ approaches the $t_{\phi,\max}$. One of the reason is that the amplitude T^{pn} contain a factor $\exp(b\tilde{t}^{pn}/2)$, which shows the same t_ϕ dependence as the single scattering amplitude and becomes large as t_ϕ goes close to $t_{\phi,\max}$. In addition to this, we note that the magnitude of the $pn \to pn$ amplitude T_2^{pn}

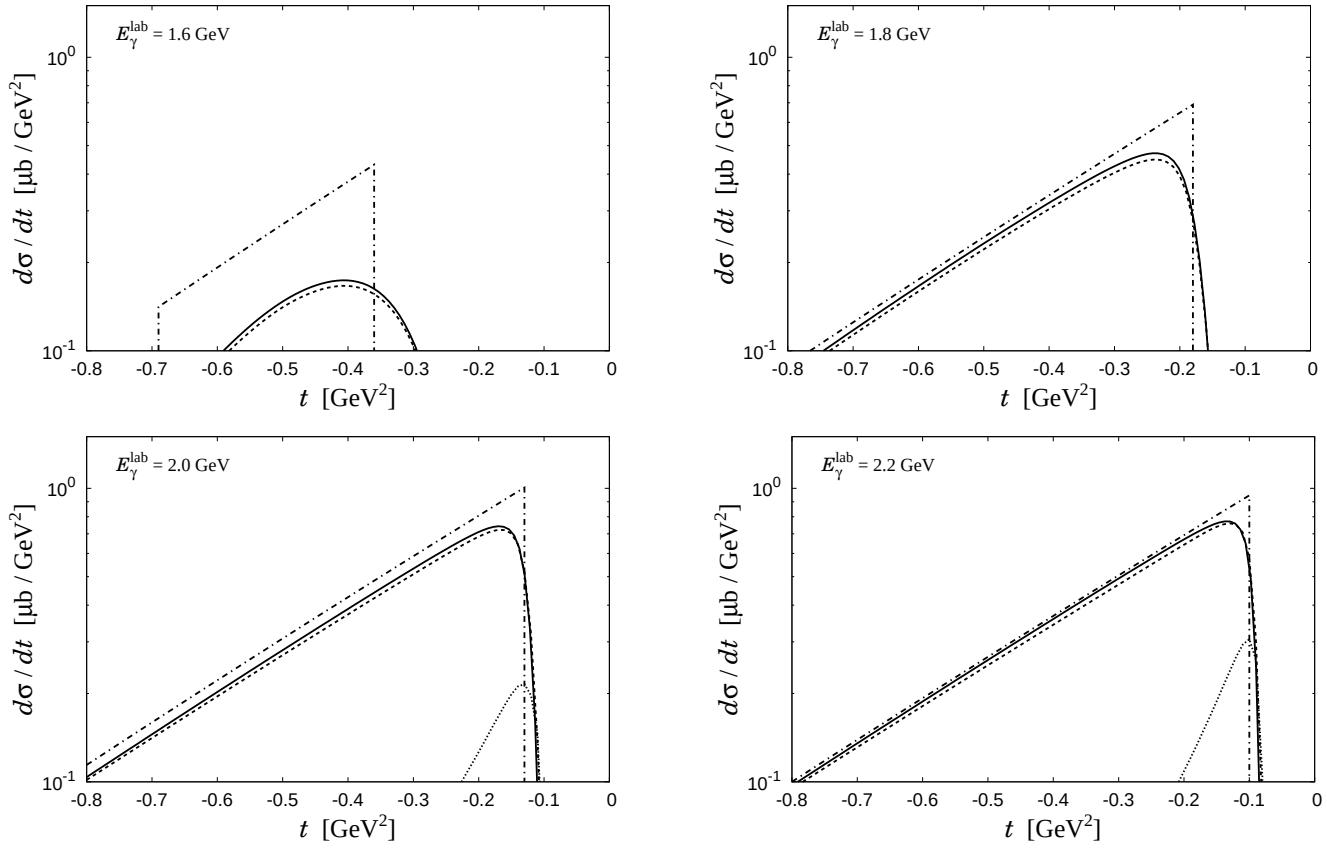

Fig. 7. Differential cross sections $d\sigma_p/dt$ and $d\sigma_{p^*}/dt_\phi$ as functions of t (t_ϕ) for different $E_\gamma^{\rm lab}$. Solid, dashed, and dotted lines indicate the single, single plus two double scatterings (ϕ and proton exchanges), and only proton-exchange scattering case of the deuteron target, and dash-doted line the case of the free proton target, respectively.

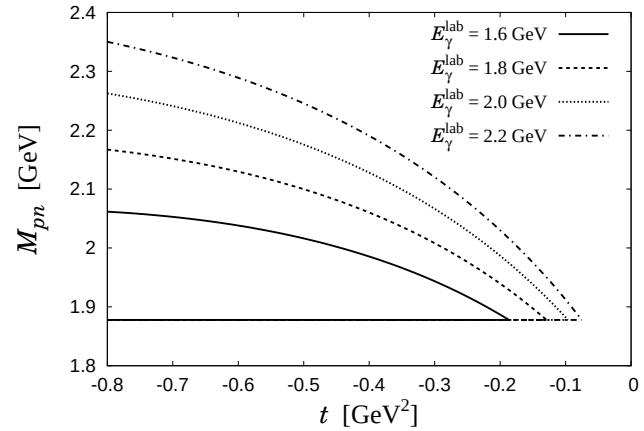

Fig. 8. Maximal and minimal values of the achievable p-n invariant mass M_{pn} for the $\gamma d \to \phi pn$ reaction in each photon energy.

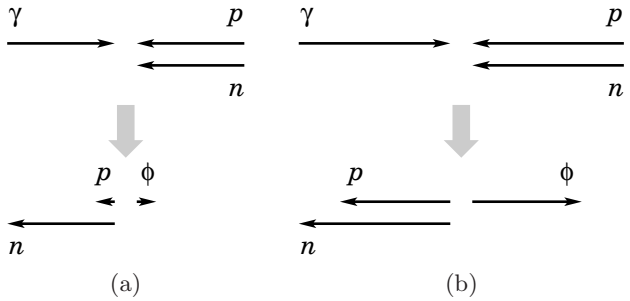

Fig. 9. Kinematics for the $\gamma d \to \phi pn$ reaction at $t_\phi \simeq t_{\phi,\max}$ with (a) photon energy close to the ϕ photoproduction threshold, and (b) appropriately large photon energy. Length of the arrows corresponds to magnitude of momenta.

gets large for $t_\phi \to t_{\phi,\max}$. This is because, in the region $t_\phi \simeq t_{\phi,\max}$ the p-n invariant mass M_{pn} is very close to the threshold $M_p + M_n$, as one can see from Fig. 8, in which the maximal as well as the minimal values of the achievable M_{pn} for fixed t_ϕ in each photon energy are plotted. Since the cross section grows rapidly as the p-n invariant mass gets close to the threshold [26] and the $pn \to pn$ amplitude is determined from the $pn \to pn$ cross section as in Eqs. (60) and (61), the $pn \to pn$ scattering amplitude also grows rapidly as the invariant mass M_{pn} approaches the threshold, or equivalently t_ϕ gets close to $t_{\phi,\max}$.

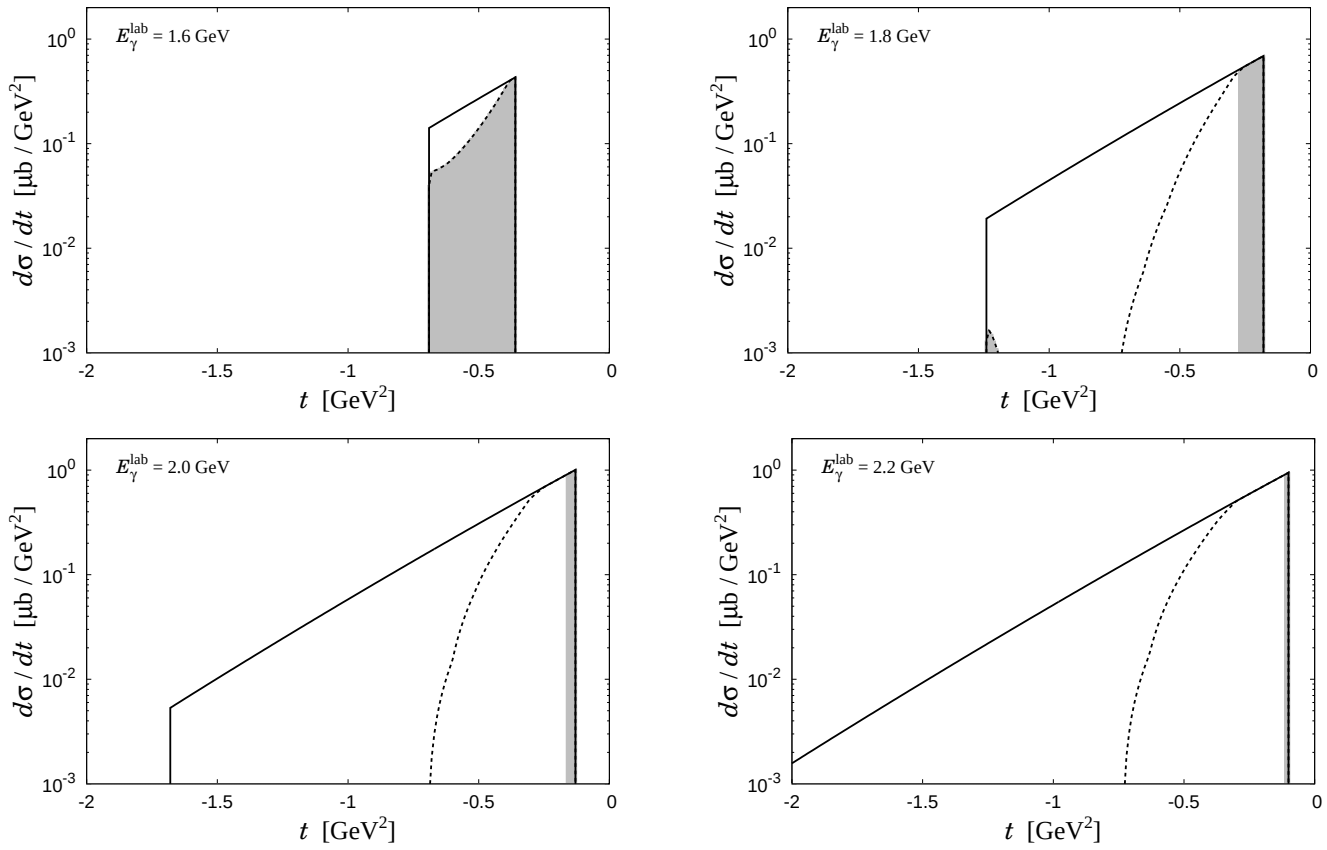

Fig. 10. Differential cross section $d\sigma_p/dt$ as a function of t for different $E_\gamma^{\rm lab}$. The solid and dashed lines, and shaded area indicate the case without any angular cuts, with the ϕ cut, and with the ϕ and proton cuts, respectively.

We also note that the proton rescattering effect increases as the photon energy increases. The reason why this occurs is that the difference between $t_{\phi,\rm max}$ and $t_{\rm max}$, the highest value of $t = (p_\phi - k)^2$ for the free proton target case, becomes small (as one can see from Fig. 5) and hence M_{pn} (t_ϕ) can easily go close to the threshold $M_p + M_n$ ($t_{\phi,\rm max}$) without help by the Fermi motion. In order to see this, we schematically show the reaction kinematics for $\gamma p^* \to \phi p$ with $t_\phi \simeq t_{\rm max}$ in the photon-bound proton center-of-mass frame in Fig. 9, where the Fermi motion is neglected. For the photon energy close to the ϕ photoproduction threshold [Fig. 9(a)], M_{pn} is large at $t_\phi \simeq t_{\rm max}$ because after the reaction the neutron momentum is large while the proton momentum is small in the photon-bound proton center-of-mass frame. In this photon energy region, one can go close to the threshold $M_{pn} \to M_p + M_n$ ($t_\phi \to t_{\phi,\rm max}$) by the help of high momentum components of the Fermi motion. For higher photon energy [Fig. 9(b)], on the other hand, M_{pn} is very close to the threshold at $t_\phi \simeq t_{\rm max}$ because the neutron and proton momenta after the reaction are very similar to each other. Hence, in this photon energy region one can go close to the threshold $M_{pn} \to M_p + M_n$ ($t_\phi \to t_{\phi,\rm max}$) without large momenta of the Fermi motion compared to the photon energy close to the ϕ photoproduction threshold. This means that the proton rescattering contribution becomes large as the photon energy becomes higher as shown in the dotted line in Fig. 7, recalling that the $pn \to pn$ amplitude gets much larger if one approaches the threshold, $M_{pn} \to M_p + M_n$ ($t_\phi \to t_{\phi,\rm max}$).

3.3 Angular cuts for charged particles

In the previous subsection we have shown the differential cross sections for the reactions $\gamma p \to \phi p$ and $\gamma d \to \phi pn$. In the LEPS experiments these reactions are identified by detecting charged particles by the spectrometer in the forward angles in the laboratory frame. Hence, let us now perform the angular cuts for the charged particles in the evaluation of the cross section such that we can compare with the LEPS experiment.

We take the angular cuts so as to keep $\Theta \leq 20$ degrees, where Θ is the angle between the momenta of the incident photon and the charged particle in the laboratory frame.

In our study, the charged particles to which we should apply the cut are the final proton and K^+K^-, which come from ϕ decay. For the proton angular cut, we can simply restrict the final state phase-space so that the final proton comes into the angle $\Theta \leq 20$ degrees. We refer to this cut as the proton cut. For the K^+ and K^- angular cuts, on the other hand, one needs some consideration, since we

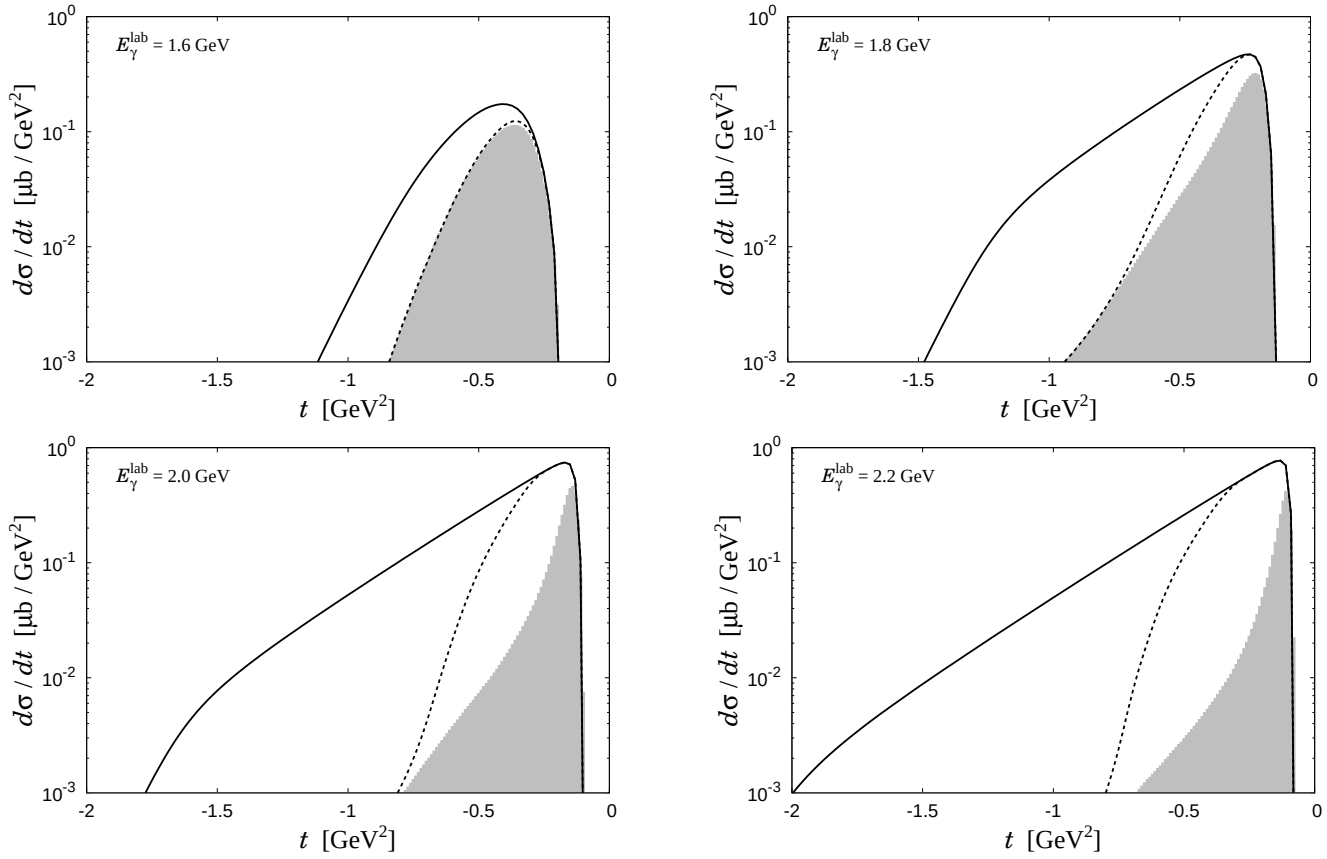

Fig. 11. Differential cross section $d\sigma_{p^*}/dt_\phi$ for a bound proton in the deuteron as a function of t_ϕ for different $E_\gamma^{\rm lab}$. The solid and dashed lines, and shaded area indicate the case without any angular cuts, with the ϕ cut, and with the ϕ and proton cuts, respectively.

do not explicitly have the final K^+ and K^-, but we have the ϕ. Here we choose the following method for the K^+ and K^- angular cuts; in each event we assume that the K^+ and K^- go out with spherical symmetry in the ϕ rest frame with momentum $\simeq 127$ MeV/c, regardless of the polarization of the ϕ. Next, we perform the Lorentz boost from the ϕ rest frame to the laboratory frame and evaluate the probability that both the K^+ and K^- come into the angle $\Theta \leq 20$ degrees. Then we multiply by this probability the cross sections in order to reproduce the K^+ and K^- angular cuts. We refer to this as the ϕ cut.

Now we show the angle-cut differential cross section for the $\gamma p \to \phi p$ reaction, $d\sigma_p/dt$, in Fig. 10. First of all, one can see that the ϕ cut suppresses $d\sigma_p/dt$ in the large $|t|$ region at any photon energies. For the region close to $t = t_{\rm max}$, however, $d\sigma_p/dt$ is not affected by the ϕ cut at any photon energy, because in this region the ϕ goes in the forward direction in the laboratory frame with sufficiently large momentum[1]. Hence, the LEPS experiment can detect the whole ϕ photoproduction events in the region close to $t = t_{\rm max}$.

Then, one can see that the proton cut does not change $d\sigma_p/dt$ at $E_\gamma^{\rm lab} = 1.6$ GeV. This is because this photon energy is very close to the threshold for the ϕ photoproduction so that the final proton, which is almost at rest in the center-of-mass frame, can come into the $\Theta \leq 20$ degrees without large transverse momentum.

The proton cut produces changes in $d\sigma_p/dt$ for photon energy bigger than $E_\gamma^{\rm lab} \simeq 1.8$ GeV. The cut produces null cross section in the middle of the $|t|$ region, that is the region where the final proton does not go forward nor backward in the center-of-mass frame. In this region the final proton has large transverse momentum, and, hence, the proton goes out of the spectrometer in the LEPS experiment. In the case that the ϕ goes forward in the center-of-mass frame, the proton cut has no effects, since the final proton goes backward in the center-of-mass, so the Lorentz boost from the center-of-mass frame to the laboratory frame keeps the proton inside the angle $\Theta \leq 20$ degrees. We should note that as $E_\gamma^{\rm lab}$ increases, the region with null cross section that the proton cut produces becomes larger, since the maximal value of the transverse momentum of the final proton also increases.

[1] Note that both the K^+ and the K^- come into the angle $\Theta \leq 20$ degrees if the ϕ has sufficiently large momentum in the forward direction in the laboratory frame, since the transverse momenta of the kaons coming from ϕ decay in the ϕ rest frame are restricted to less than 127 MeV/c.

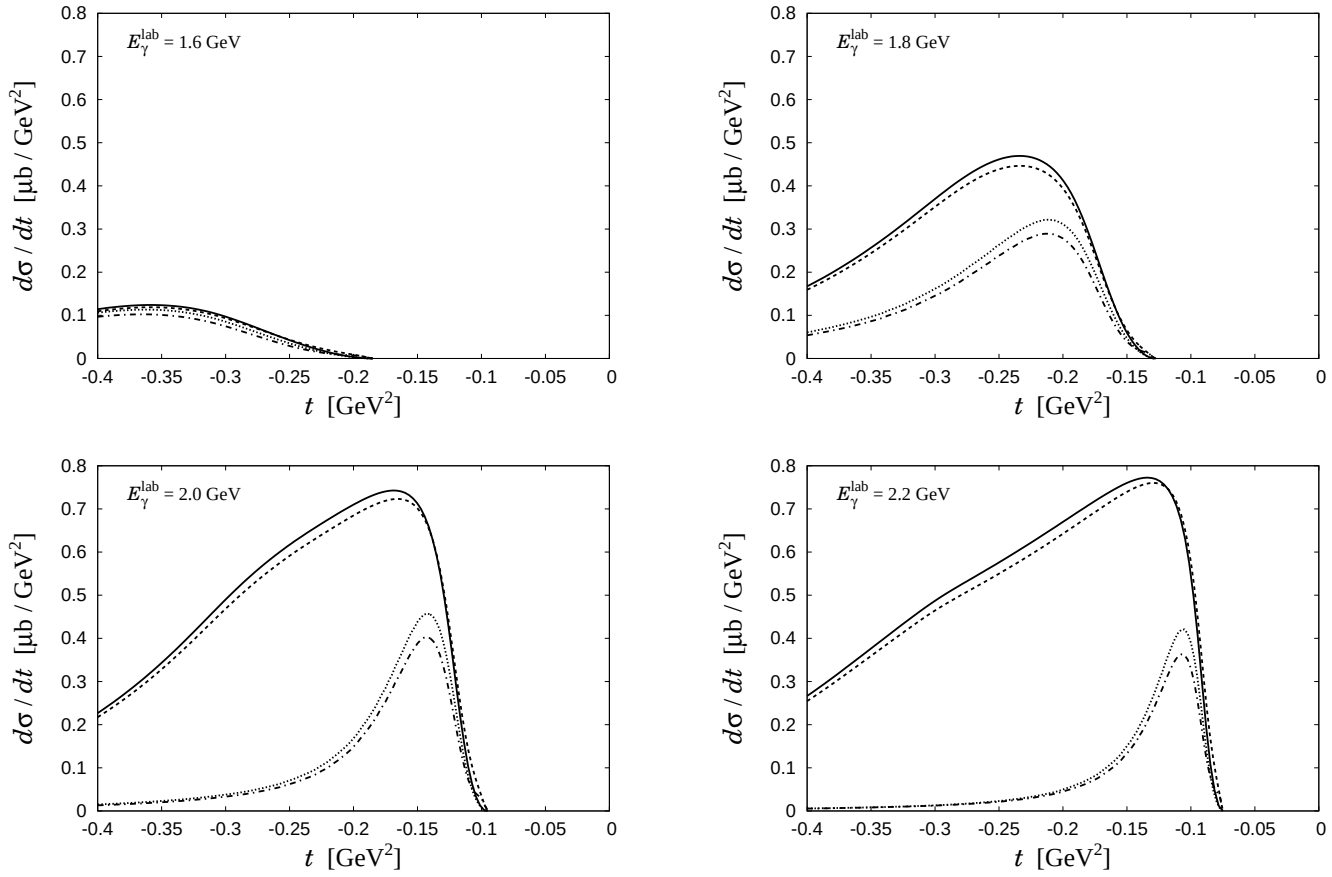

Fig. 12. Differential cross section $d\sigma_{p^*}/dt_\phi$ for a bound proton in the deuteron as a function of t_ϕ for different $E_\gamma^{\rm lab}$. The solid and dashed lines indicate single scattering and single plus two double scattering (ϕ and proton exchanges) contributions, respectively, with only ϕ cut. The dotted and dash-dotted lines indicate single scattering and single plus two double scattering (ϕ and proton exchanges) contributions, respectively, with both ϕ and proton cuts.

For the free proton target $\gamma p \to \phi p$ reaction, however, one does not need to detect the final proton by the spectrometer; in this reaction one can identify the final proton by using the missing mass method. Therefore, the proton cut is not implemented in the experiments in this reaction and theoretically we should calculate $d\sigma_p/dt$ only with the ϕ cut. As one can see, only with the ϕ cut $d\sigma_p/dt$ is suppressed in the large $|t|$ region, whereas it is not affected in the region close to $t = t_{\rm max}$. Should one wish to obtain $d\sigma_p/dt$ experimentally for the case without angular cuts, one should make acceptance corrections, which were done in [15].

Now let us show the effects of the angular cut on the $\gamma d \to \phi pn$ reaction in Fig. 11, where only the single scattering is taken into account. One of the important features from Fig. 11 is that at any photon energy the ϕ cut does not produce changes in the cross section in the region close to $t_\phi = t_{\phi,\rm max}$, like in the $\gamma p \to \phi p$ case, whereas the ϕ cut changes the cross section in the large $|t_\phi|$ region. This suggests that all of the K^+K^- from the ϕ can go into the LEPS spectrometer in the region close to $t_\phi = t_{\phi,\rm max}$.

The proton cut effects, on the other hand, appear above the photon energy $E_\gamma^{\rm lab} \simeq 1.8$ GeV. This proton cut, however, does not completely suppress $d\sigma_{p^*}/dt_\phi$, as it was the case in the $\gamma p \to \phi p$ reaction. The finite $d\sigma_{p^*}/dt_\phi$ with the proton cut is caused by the Fermi motion in the deuteron bound system. This $d\sigma_{p^*}/dt_\phi$ suppression due to the proton cut gets bigger as the photon energy increases, the same as for the $\gamma p \to \phi p$ reaction.

It is important to keep in mind this suppression created by the proton cut. Namely, in the $\gamma d \to \phi pn$ reaction in the LEPS experiment the $\gamma p^* \to \phi p$ reaction is identified by detecting also the final proton in addition to the K^+K^- in the spectrometer. Since the double scattering mechanism of Fig. 3(b) contributes scarcely to $d\sigma_{p^*}/dt_\phi$ in the small $|t_\phi|$ region (see Fig. 5) and the Fermi motion of the neutron is moderate in the deuteron, one can identify the $\gamma p^* \to \phi p$ process in the deuteron by detecting relatively fast protons. However, in order to compare $d\sigma_{p^*}/dt_\phi$ for photoproduction on a proton in the deuteron with $d\sigma_p/dt$, one has to consider the proton cut effects on $d\sigma_{p^*}/dt_\phi$ and has to perform the acceptance correction for the proton cut in addition to that for the ϕ cut. These acceptance corrections are done in the experiment, although no details are given in the paper. In view of the strong t_ϕ

dependence of the proton cut, details on how the acceptance corrections are done would be most advisable.

Next let us examine the angular cut effects on the double scattering contributions. The effects of the ϕ and the proton cuts are shown in Fig. 12. As one can see from Fig. 12, the two double scattering (ϕ and proton exchanges) contributions with the ϕ cut do not largely suppress the contribution from the single scattering (solid and dashed lines). However, if the proton cut is taken into account the two double scattering contributions suppress the differential cross section compared to that with only the single scattering in a larger amount than if only the ϕ cut is considered, especially in $t_\phi \simeq t_{\phi,\max}$ region (dotted and dash-dotted lines). Remembering that the ϕ rescattering effect is small at $t_\phi \simeq t_{\phi,\max}$, this suppression originates from the proton rescattering effect.

Since the proton cut is important for the suppression of $d\sigma_{p^*}/dt_\phi$, the suppression behavior can be interpreted as follows: namely, the final proton in forward angle is rescattered by the neutron and the proton direction changes. Then the number of protons in the forward direction decreases, and this is taken into account by the imaginary part of the $pn \to pn$ amplitude T_2^{pn}. The proton in this collision is not lost, but it is simply redistributed in other directions. Technically we saw that this was accomplished by means of the real part of the $pn \to pn$ amplitude T_2^{pn}. Then, due to the proton cut in the $t_\phi \simeq t_{\phi,\max}$ region, some of these protons will not reach the LEPS detector. Furthermore, the proton rescattering effect of forward to another angle for the proton is larger than that of another angle to forward for the proton and we see a net suppression of forward going protons.

In order to see how much the double scattering effects suppress $d\sigma_{p^*}/dt_\phi$ compared to the single scattering contribution, we show the ratio of the differential cross sections with the three contributions to that with only single scattering in Fig. 13. In Fig. 13, both the ϕ and proton cuts are performed. From the figure, one can see that the double scattering effects suppress the cross section, especially in the $t_\phi \sim t_{\phi,\max}$ region, about to 85% regardless of the initial photon energy. The ratio is close to 90% if a bin of $\Delta t = 0.1$ GeV^2 is taken, as in [31]. This small reduction goes in the direction reported in [17] for the ratio of ϕ photoproduction on a bound proton inside the deuteron to the one on a free proton, but is short of the value around 60% reported there for large energies. The rapid increase of the ratio at $t_\phi \simeq t_{\phi,\max}$ shown in Fig. 13 is caused by the threshold effect for t_ϕ and gives no trouble in the differential cross sections themselves.

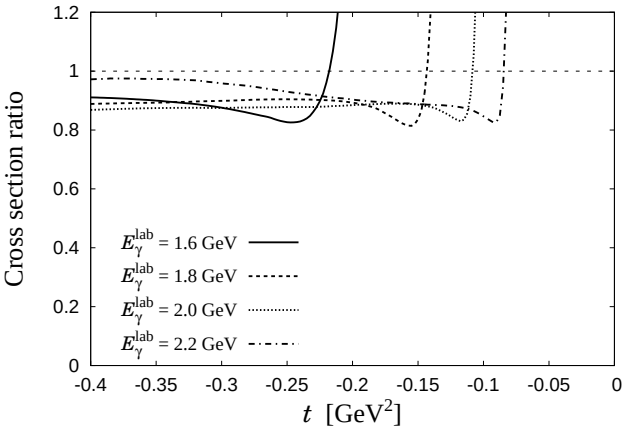

Fig. 13. Ratio of the differential cross sections $d\sigma_{p^*}/dt_\phi$ with three contributions (single scattering and ϕ- and proton-exchange amplitudes) to that only with single scattering. Both ϕ and proton angle cuts are performed.

3.4 Ratio of the cross sections

Now that we have all the results, we try to compare the ratio of the differential cross sections, $(d\sigma_{p^*}/dt_\phi)/(d\sigma_p/dt)$ from LEPS experiments [17] with the theoretical results.

In the LEPS experiment, they found a significant diversion with respect to unity (see Fig. 4 of Ref. [17]). There they detect the K^+K^-p in the $\gamma d \to \phi pn$ reaction so as to identify the $\gamma p^* \to \phi p$ in the deuteron and evaluate the ratio of this cross section to the one on the free proton.

From the theoretical point of view the comparison of $d\sigma/dt$ for the proton in the deuteron and the free proton can be obtained from the ratio of the dashed line and dashed-dotted line in Fig. 7 for each energy. This is leaving apart the effect of the ϕ and proton cuts discussed above, from where one can expect a reduction of 10% in the ratio. Of course, one can see that as one approaches $t_{\max}$, the ratio changes very fast from values around 0.8 close to $t_{\max}$, to around 0.4 at $t_{\max}$. The ratio becomes infinity if we go a bit beyond $t_{\max}$, since the reaction is forbidden in the free case, but is allowed in the deuteron due to the Fermi motion.

However, we cannot compare these results with those obtained in Fig. 4 of Ref. [17], the reason being that the experimental paper does not provide enough information to allow for a meaningful comparison. We hope that an extended version of the concise information given in [17] can provide these needed details. In order to facilitate this task we write below the information that we would need for a proper comparison.

1) How and where is the deuteron wave function taken into account to remove effects of Fermi motion in [17], if this is the case?
2) In Fig. 4 of [17] $E_\gamma^{\rm eff}$ is used in the x axis without any comment or definition. We assume that this is not a misprint, but that indeed the concept of $E_\gamma^{\rm eff}$ introduced in [32] is used there[2]. This concept relies upon the MMSA (minimum momentum spectator approximation) which approximates the spectator nucleon momentum as the minimum one without specifying whether it is a proton or a neutron (see also the repercussion of its use in the analysis of the "Θ^+" peak as discussed in [33]). It is important that the details on

[2] This seems to be the case according to the private communication [31].

the use of this prescription in the present analysis are provided.

3) When dealing with Fermi motion close to $t_{\rm max}$, the binning of Δt used to determine $d\sigma_{p^*}/dt$ is also important, in view of the fast change of the cross section as a function of t_ϕ close to $t_{\rm max}$. On the other hand, the use of a large binning can lead to other problems of interpretation. Indeed, assume one takes $\Delta t = 0.1$ GeV^2, then for events with $t_\phi = t_{\rm max} - \Delta t$, $d\sigma_{p^*}/dt$ has already fallen to 70% of the value at $t_{\rm max}$, as given by Eq. (9). Similarly, as seen in Fig. 11, the effect of the proton angle cut at the highest energy $E_\gamma^{\rm lab} = 2.2$ GeV leads to a reduction of $d\sigma_{p^*}/dt$ at $t_\phi = t_{\rm max} - \Delta t$ to about 31% of its value at $t_{\rm max}$. The combined effect of the two would be a reduction by a factor of about 0.1 at $\Delta t = 0.1$ GeV^2.
4) Although methods could be devised to eliminate the contribution to the "proton in deuteron" cross section from the unwanted case where the proton is a spectator, it should be kept in mind that the Fermi motion provides a distribution of momenta to these spectator protons, some of which could be observed and be misidentified as participant protons. Details on how this problem is avoided would also be most welcome.
5) At some point in the experimental analysis, knowing the proton momentum will be important. How this momentum is reconstructed from the observed events in view of the expected distortion caused by the target in the detected protons is also a relevant information. This point becomes more critical once we have shown that the proton angular cuts are so relevant for the cross section close to $t_{\rm max}$. Furthermore, in view of the losses in the detection of protons, when the K^+ and K^- are detected in coincidence, one should also clarify the statistical situation of these events and how $d\sigma_{p^*}/dt$ is obtained in this case, providing statistical and systematic errors.

When this information is provided, we could continue our work with a meaningful comparison with the data of [17]. At the present time, this comparison, and the interpretation of the data from our theoretical perspective is not possible. Yet, we found that the consideration of proton rescattering in the deuteron, together with the effect of the proton cut, can produce a moderate reduction of the medium to free proton ϕ photoproduction cross section of about 10%, which goes in the direction reported in [17], but falls short of the numbers quoted there.

4 Summary

We have done a study of ϕ photoproduction on the proton and on the deuteron, and in particular on a proton in the deuteron, using an accurate wave function for the deuteron that accounts for the Fermi motion, which we found to be very important when studying $d\sigma/dt$ close to $t_{\rm max}$. We also took into account rescattering of the ϕ including the mechanisms that lead to ϕ absorption and provide realistic values of the ϕ width in a nuclear medium. We found that the latter mechanisms are very small. The screening of the ϕ production in the deuteron is found to be very small. This could be consistent with moderate changes of the screening of the ϕ production seen in nuclei [19,38, 39]. This conclusion is in agreement with the recent experiment at Jefferson Lab. [24] where the extracted $d\sigma/dt$ is consistent with predictions based on the quasifree mechanism.

We studied in detail the effects of the ϕ and proton cuts to accommodate the theoretical results to the measurements of LEPS, taking into account the LEPS set up which restricts the detected particles to forward angles. We found that the proton cut, which does not appear in the free proton case, because its momentum is reconstructed from the K^+ and K^- momenta, plays an important role in the scattering on the deuteron since protons are detected in this case. The largest effect, even then rather moderate, was the about 10% reduction in the ratio of medium to free proton photoproduction cross sections that we obtain from the consideration of proton rescattering in the deuteron, together with the ϕ and proton cuts of the LEPS set up implemented in both of them to provide a proper comparison.

Finally, we discussed that a comparison of our results with the experimental ones provided in [17] was not possible at the present stage due to the absence of relevant experimental information in [17]. We suggested that a more detailed experimental paper be written and we listed the experimental information that would be needed for a meaningful comparison in the future.

Acknowledgements

This work is supported in part by the Grant-in-Aid for Scientific Research from MEXT and JSPS (Nos. 22105507, 22740161, and 22-3389), the Bilateral International Exchange Program (BIEP) of the Global COE Program "The Next Generation of Physics, Spun from Universality and Emergence" from MEXT of Japan, and the collaboration agreement between the JSPS of Japan and the CSIC of Spain. This work is partly supported by DGICYT contract number FIS2006-03438 and the Generalitat Valenciana in the program Prometeo. We acknowledge the support of the European Community-Research Infrastructure Integrating Activity "Study of Strongly Interacting Matter" (acronym HadronPhysics2, Grant Agreement n. 227431) under the Seventh Framework Programme of EU. One of the authors (T.S.) acknowledges the support by the Grand-in-Aid for JSPS fellows. This work is partially done under the Yukawa International Program for Quark-hadron Sciences (YIPQS).

A $\phi n \to \phi n$ scattering amplitude

In this Appendix we evaluate the $\phi n \to \phi n$ scattering amplitude. Since we are concerned about the absorptive imaginary part of this amplitude, we take into account

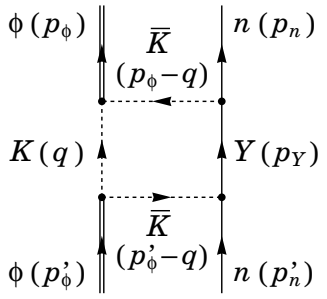

Fig. 14. Box diagram for $\phi n \to \phi n$ reaction together with momentum of each particle. The channels of K, $\bar{K}$, and Y are given in Tab. 1.

Table 1. Channels of K, $\bar{K}$, and Y appearing in Fig. 14. The Clebsch-Gordan coefficients α, β, and A are also shown.

Channel	K	$\bar{K}$	Y	α	β	A
1	K^+	K^-	Σ^-	0	$\sqrt{2}$	–
2	K^+	K^-	Σ^{*-}	–	–	-1
3	K^0	$\bar{K}^0$	Λ	$-2/\sqrt{3}$	$1/\sqrt{3}$	–
4	K^0	$\bar{K}^0$	Σ^0	0	-1	–
5	K^0	$\bar{K}^0$	Σ^{*0}	–	–	$1/\sqrt{2}$

here the same mechanisms that were considered in the evaluation of the width of the ϕ in the medium in [34, 35]. These are depicted in Figs. 14 (the box diagram) and 15 (the vertex corrections). Here Y denotes the Λ, Σ and $\Sigma(1385)$ (Σ^*) hyperons.

First, we consider the box diagram (Fig. 14) with Λ and Σ propagation, which is evaluated as,

$$
\begin{aligned}
&-iT^{\Lambda,\,\Sigma}_{\phi n\to\phi n}\\
&=\sum_{\Lambda,\,\Sigma}\int\frac{d^4q}{(2\pi)^4}\frac{i}{q^2-m_K^2+i\epsilon}\frac{i}{(p_\phi-q)^2-m_{\bar{K}}^2}\\
&\quad\times\frac{i}{(p'_\phi-q)^2-m_{\bar{K}}^2}[-ig_\phi\epsilon^*_\mu(\phi)(2q-p_\phi)^\mu]\\
&\quad\times\tilde{V}\boldsymbol{\sigma}\cdot(\boldsymbol{q}-\boldsymbol{p}_\phi)\frac{iM_Y/E_Y(|\boldsymbol{p}'_n+\boldsymbol{p}'_\phi-\boldsymbol{q}|)}{p'^0_n+p'^0_\phi-q^0-E_Y(|\boldsymbol{p}'_n+\boldsymbol{p}'_\phi-\boldsymbol{q}|)+i\epsilon}\\
&\quad\times[-ig_\phi\epsilon_\nu(\phi)(2q-p'_\phi)^\nu]\tilde{V}\boldsymbol{\sigma}\cdot(\boldsymbol{p}'_\phi-\boldsymbol{q}),
\end{aligned}
\tag{63}
$$

where M_Y is the mass of the hyperon propagating in the intermediate state, and $E_Y(p)=\sqrt{M_Y^2+p^2}$. The summation symbol with subscripts Λ and Σ represents the sum of the contribution from Λ and Σ propagation in the intermediate states. These channels are explicitly given in Tab. 1. The $\phi K\bar{K}$ coupling constant is denoted by g_ϕ and is fixed as $g_\phi = 4.57$ so as to reproduce the decay width for $\phi\to K\bar{K}$. In Eq. (63) $\boldsymbol{\sigma}$ are Pauli matrices for baryon spin. The quantity $\tilde{V}$ is the coefficient for the meson-baryon-baryon coupling fixed by the flavor $SU(3)$ symmetry as,

$$
\tilde{V}=\alpha\frac{D+F}{2f}+\beta\frac{D-F}{2f},
\tag{64}
$$

with empirical parameters $D+F=1.26$, $D-F=0.33$, and $f=1.15f_\pi$ with the pion decay constant $f_\pi = 93.0\,\mathrm{MeV}$. The magnutides α and β correspond to $SU(3)$ Clebsch-Gordan coefficients and are shown in Tab. 1.

In the double scattering diagram of Fig. 3, $\boldsymbol{p}'_\phi=\boldsymbol{q}_{\rm ex}$. If we consider ϕ production forward, as in the experiment, $\boldsymbol{p}_\phi$ and $\boldsymbol{p}'_\phi$ will be forward and $\boldsymbol{p}_n$ and $\boldsymbol{p}'_n$ will be small. Therefore, we can approximate the amplitude substituting $\boldsymbol{q}_{\rm ex}$ by $\boldsymbol{p}_\phi$, in which case $\boldsymbol{p}_n\simeq\boldsymbol{p}'_n\simeq\boldsymbol{0}$. We also discussed in Sect. 2.2.2 that we were interested in the case where the polarization of the initial and final ϕ were the same, to optimize the interference of $T^{\rm ds}$ with $T^{\rm ss}$. Hence, we can take the average amplitude over the ϕ polarizations for which we use,

$$
\overline{\sum_{\lambda_\phi}}\epsilon^*_\mu(\phi)(2q-p_\phi)^\mu\epsilon_\nu(\phi)(2q-p_\phi)^\nu=\frac{4}{3}\left[\frac{(p_\phi\cdot q)^2}{M_\phi^2}-q^2\right].
\tag{65}
$$

Note that the approximation done also forces the neutrons to have the same polarization since,

$$
[(\boldsymbol{q}-\boldsymbol{p}_\phi)\cdot\boldsymbol{\sigma}][(\boldsymbol{p}_\phi-\boldsymbol{q})\cdot\boldsymbol{\sigma}]=-|\boldsymbol{q}-\boldsymbol{p}_\phi|^2,
\tag{66}
$$

and there is no spin flip term. The independence of this amplitude on the spin of the second particle is of relevance to our approach. Indeed, we have used a ϕ photoproduction amplitude on the first nucleon which is independent of the spin of the nucleon. If we had a spin dependent amplitude the spin structure of the deuteron should in principle be taken into account. However, if there is only spin dependence on the first nucleon, the sum over initial and final polarization for the case of initial nucleons uncorrelated by spin, as we have assumed, or correlated in a spin = 1 (or zero) state as in the deuteron, give the same result.

The imaginary part of $T^{\Lambda,\,\Sigma}_{\phi n\to\phi n}$ in Eq. (63) is readily evaluated using the Cutkosky rules suited to our normalization as in [36],

$$
T^{\Lambda,\,\Sigma}_{\phi n\to\phi n}\to 2i\mathrm{Im}T^{\Lambda,\,\Sigma}_{\phi n\to\phi n},\quad G(q)\to 2i\theta(q^0)\mathrm{Im}G(q),
\tag{67}
$$

with G the propagators of the particles which are placed on the mass-shell, in the present case, the K and Y of Fig. 14. Hence, we obtain,

$$
\begin{aligned}
\mathrm{Im}T^{\Lambda,\,\Sigma}_{\phi n\to\phi n}&=-\frac{1}{2}\sum_{\Lambda,\,\Sigma}\int\frac{d^3q}{(2\pi)^3}\frac{1}{2\omega(|\boldsymbol{q}|)}\frac{M_Y}{E_Y(|\boldsymbol{p}_\phi+\boldsymbol{p}_n-\boldsymbol{q}|)}\\
&\quad\times|\mathcal{T}_1|^2\times 2\pi\delta(p^0_\phi+p^0_n-E_Y(|\boldsymbol{p}_\phi+\boldsymbol{p}_n-\boldsymbol{q}|)-\omega(|\boldsymbol{q}|))
\end{aligned}
\tag{68}
$$

with $\omega(q)=\sqrt{m_K^2+q^2}$ and,

$$
|\mathcal{T}_1|^2=\frac{4}{3}\left(\frac{g_\phi\tilde{V}|\boldsymbol{q}-\boldsymbol{p}_\phi|}{M_\phi^2-2p_\phi\cdot q}\right)^2\times\left[\frac{(p_\phi\cdot q)^2}{M_\phi^2}-m_K^2\right],
\tag{69}
$$

where we have used $q^2=m_K^2=m_{\bar{K}}^2$.

We can see that Eq. (68) is the phase-space integral for the cross section of $\phi n\to KY$ with the transition amplitude $\mathcal{T}_1$ up to a normalization. Performing explicitly the

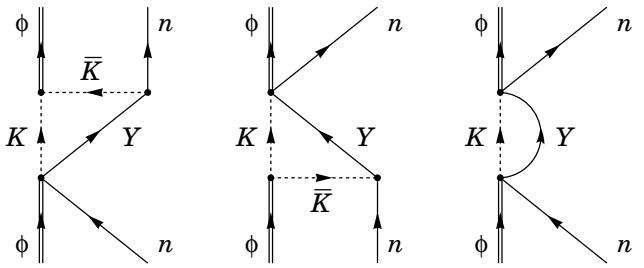

Fig. 15. Diagrams for the vertex corrections of $\phi n \to \phi n$ reaction. The channels of K, $\bar{K}$, and Y are given in Tab. 1.

$|\boldsymbol{q}|$ integration in the ϕ-n center-of-mass frame we obtain,

$$\mathrm{Im}\, T^{\Lambda,\,\Sigma}_{\phi n\to\phi n} = -\sum_{\Lambda,\,\Sigma}\frac{|\boldsymbol{q}|M_Y}{8\pi M_{\phi n}}\int_{-1}^{1} d\cos\theta_K |\mathcal{T}_1|^2, \qquad (70)$$

with $M_{\phi n} = \sqrt{(p_\phi + p_n)^2}$ and θ_K the scattering angle between the ϕ and the K. Eq. (70) is nothing but the expression of the optical theorem for the reaction mechanism of Fig. 14.

Next we consider the vertex corrections diagrams of the $\phi n \to \phi n$ amplitude shown in Fig. 15 with the Λ and Σ propagation [34]. Following [37], we obtain for the sum of the three diagrams the same expression for $\mathrm{Im}T^{\Lambda,\,\Sigma}_{\phi n\to\phi n}$ in Eq. (70), substituting $|\mathcal{T}_1|^2$ by $|\mathcal{T}_2|^2$ given by[3],

$$|\mathcal{T}_2|^2 = (g_\phi \tilde{V})^2 \times\left[\frac{4}{3}\frac{1}{M_\phi^2 - 2p_\phi\cdot q}\left(|\boldsymbol{q}|^2 - \boldsymbol{p}_\phi\cdot\boldsymbol{q} + \frac{p_\phi\cdot q}{M_\phi^2}(|\boldsymbol{p}_\phi|^2 - \boldsymbol{p}_\phi\cdot\boldsymbol{q})\right) + \left(1 + \frac{|\boldsymbol{p}_\phi|^2}{3M_\phi^2}\right)\right]. \qquad (71)$$

For the contributions with the Λ and Σ propagation in Figs. 14 and 15, summing Eqs. (69) and (71), we obtain,

$$\mathrm{Im}\, T^{\Lambda,\,\Sigma}_{\phi n\to\phi n} = -\sum_{\Lambda,\,\Sigma}\frac{|\boldsymbol{q}|M_Y}{8\pi M_{\phi n}}\int_{-1}^{1} d\cos\theta_K (|\mathcal{T}_1|^2 + |\mathcal{T}_2|^2). \qquad (72)$$

Now let us consider Σ^* propagation. The amplitude with the Σ^* propagation can be obtained by replacement of the coupling constant, spin matrix and mass in the amplitudes obtained for the Λ and Σ propagations. The coupling constant for Σ^* is obtained by an $SU(6)$ quark model and $SU(3)$ flavor symmetry as,

$$\tilde{V} \to \tilde{A} = \frac{2\sqrt{6}}{5}\frac{D+F}{2f}A, \qquad (73)$$

with the Clebsch-Gordan coefficient A given in Tab. 1. The spin operators in the case of the Σ^* are the transition matrices of spin 1/2 to 3/2, $\boldsymbol{S}^\dagger$, which should be used instead of the Pauli matrices $\boldsymbol{\sigma}$, and they satisfy the relation,

$$S^i S^{\dagger j} = \frac{2}{3}\delta^{ij} - \frac{i}{3}\epsilon_{ijk}\sigma^k, \qquad (74)$$

This gives an extra factor 2/3 since the spin flip part vanishes in the equivalent term of Eq. (66). Finally, we obtain for the imaginary part of the $\phi n \to \phi n$ amplitude for the Σ^* propagation

$$\mathrm{Im}\, T^{\Sigma^*}_{\phi n\to\phi n} = -\sum_{\Sigma^*}\frac{|\boldsymbol{q}|M_Y}{12\pi M_{\phi n}}\int_{-1}^{1} d\cos\theta_K (|\mathcal{U}_1|^2 + |\mathcal{U}_2|^2), \qquad (75)$$

with,

$$|\mathcal{U}_1|^2 = \frac{4}{3}\left(\frac{g_\phi\tilde{A}|\boldsymbol{q}-\boldsymbol{p}_\phi|}{M_\phi^2 - 2p_\phi\cdot q}\right)^2 \times\left[\frac{(p_\phi\cdot q)^2}{M_\phi^2} - m_K^2\right], \qquad (76)$$

$$|\mathcal{U}_2|^2 = (g_\phi\tilde{A})^2 \times\left[\frac{4}{3}\frac{1}{M_\phi^2 - 2p_\phi\cdot q}\left(|\boldsymbol{q}|^2 - \boldsymbol{p}_\phi\cdot\boldsymbol{q} + \frac{p_\phi\cdot q}{M_\phi^2}(|\boldsymbol{p}_\phi|^2 - \boldsymbol{p}_\phi\cdot\boldsymbol{q})\right) + \left(1 + \frac{|\boldsymbol{p}_\phi|^2}{3M_\phi^2}\right)\right]. \qquad (77)$$

As a consequence, the final form for the imaginary part of the $\phi n \to \phi n$ amplitude can be written as

$$\mathrm{Im}\, T_{\phi n\to\phi n}(M_{\phi n}) = \mathrm{Im}\, T^{\Lambda,\,\Sigma}_{\phi n\to\phi n} + \mathrm{Im}\, T^{\Sigma^*}_{\phi n\to\phi n}, \qquad (78)$$

which can be readily evaluated using Eqs. (72) and (75). In Fig. 16 we show the results that we get for $\mathrm{Im}\, T_{\phi n\to\phi n}$ as a function of $M_{\phi n}$. In order to get a feeling for the results in Fig. 16, rather than calculating an inelastic cross section which goes to infinity at the ϕ-n threshold, we give the ϕ width in a nuclear medium $\Gamma = -\mathrm{Im}\, T_{\phi n\to\phi n}\rho/\omega_\phi$, with ρ the nuclear matter density. For normal nuclear matter density, $\rho_0 = 0.17$ fm^{-3}, this gives $\Gamma \simeq 27$ MeV at threshold, in agreement with the results obtained in Refs. [33, 34].

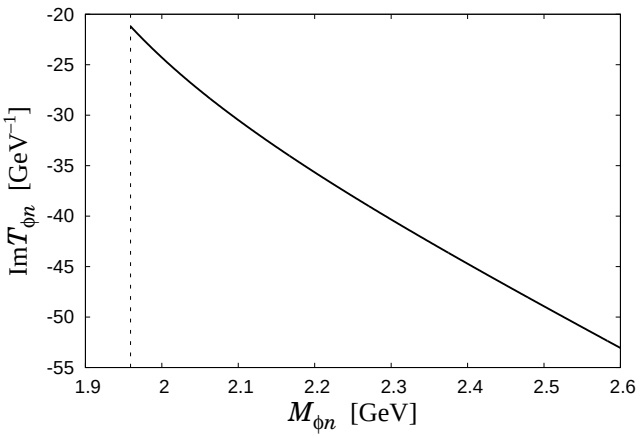

Fig. 16. $\mathrm{Im}\, T_{\phi n\to\phi n}$ as a function of $M_{\phi n}$. Vertical dashed line represents the ϕ-n threshold.

[3] We found that one should use $(1 + |\boldsymbol{p}_\phi|^2/3M_\phi^2)$ instead of $(1 + |\boldsymbol{q}|^2/3M_\phi^2)$ given as the last term of Eq. (11) in [37].

References

1. J. Ballam *et al.*, Phys. Rev. D **7** (1973) 3150.
2. H. J. Besch, G. Hartmann, R. Kose, F. Krautschneider, W. Paul and U. Trinks, Nucl. Phys. B **70** (1974) 257.
3. H. J. Behrend *et al.*, Nucl. Phys. B **144** (1978) 22.
4. D. P. Barber *et al.*, Z. Phys. C **12** (1982) 1.
5. E. Anciant *et al.* [CLAS Collaboration], Phys. Rev. Lett. **85** (2000) 4682 [arXiv:hep-ex/0006022].
6. J. Barth *et al.*, Eur. Phys. J. A **17** (2003) 269.
7. T. H. Bauer, R. D. Spital, D. R. Yennie and F. M. Pipkin, Rev. Mod. Phys. **50** (1978) 261 [Erratum-ibid. **51** (1979) 407].
8. A. I. Titov, S. N. Yang and Y. s. Oh, Nucl. Phys. A **618** (1997) 259 [arXiv:nucl-th/9612059].
9. A. I. Titov, Y. s. Oh and S. N. Yang, Phys. Rev. Lett. **79** (1997) 1634 [arXiv:nucl-th/9702015].
10. A. I. Titov, Y. s. Oh, S. N. Yang and T. Morii, Phys. Rev. C **58** (1998) 2429 [arXiv:nucl-th/9804043].
11. A. I. Titov, T. S. H. Lee and H. Toki, Phys. Rev. C **59** (1999) 2993 [arXiv:nucl-th/9812074].
12. A. I. Titov, T. S. Lee, H. Toki and O. Streltsova, Phys. Rev. C **60** (1999) 035205.
13. L. S. Kisslinger and W. h. Ma, Phys. Lett. B **485** (2000) 367 [arXiv:hep-ph/9905479].
14. F. J. Llanes-Estrada, S. R. Cotanch, P. J. de A. Bicudo, J. E. F. Ribeiro and A. P. Szczepaniak, Nucl. Phys. A **710** (2002) 45 [arXiv:hep-ph/0008212].
15. T. Mibe *et al.* [LEPS Collaboration], Phys. Rev. Lett. **95** (2005) 182001 [arXiv:nucl-ex/0506015].
16. A. I. Titov, T. Nakano, S. Date and Y. Ohashi, Mod. Phys. Lett. A **23** (2008) 2301.
17. W. C. Chang *et al.* [LEPS Collaboration], Phys. Lett. B **684** (2010) 6 [arXiv:0907.1705 [nucl-ex]].
18. A. I. Titov and B. Kampfer, Phys. Rev. C **76** (2007) 035202 [arXiv:0705.2010 [nucl-th]].
19. T. Ishikawa *et al.*, Phys. Lett. B **608** (2005) 215 [arXiv:nucl-ex/0411016].
20. E. Hernandez and E. Oset, Z. Phys. A **341** (1992) 201.
21. R. Rapp and J. Wambach, Adv. Nucl. Phys. **25** (2000) 1 [arXiv:hep-ph/9909229].
22. R. S. Hayano and T. Hatsuda, Rev. Mod. Phys. **82** (2010) 2949 [arXiv:0812.1702 [nucl-ex]].
23. V. K. Magas, L. Roca and E. Oset, Phys. Rev. C **71** (2005) 065202 [arXiv:nucl-th/0403067].
24. X. Qian, W. Chen, H. Gao, K. Hicks, K. Kramer, J. M. Laget, T. Mibe and Y. Qiang *et al.*, Phys. Lett. B **696** (2011) 338 [arXiv:1011.1305 [nucl-ex]].
25. T. C. Rogers, M. M. Sargsian and M. I. Strikman, Phys. Rev. C **73** (2006) 045202 [arXiv:hep-ph/0509101].
26. C. Amsler *et al.* [Particle Data Group], Phys. Lett. B **667** (2008) 1.
27. D. Jido, E. Oset and T. Sekihara, Eur. Phys. J. A **42** (2009) 257.
28. M. Lacombe, B. Loiseau, R. Vinh Mau, J. Cote, P. Pires and R. de Tourreil, Phys. Lett. B **101** (1981) 139.
29. R. Machleidt, Phys. Rev. C **63** (2001) 024001.
30. NN-OnLine, http://nn-online.org/
31. M. Miyabe, Doctor thesis (2010); in private communication.
32. T. Nakano *et al.* [LEPS Collaboration], Phys. Rev. C **79** (2009) 025210.
33. A. M. Torres and E. Oset, Phys. Rev. C **81** (2010) 055202 [arXiv:1003.1098 [nucl-th]].
34. E. Oset and A. Ramos, Nucl. Phys. A **679** (2001) 616.
35. D. Cabrera and M. J. Vicente Vacas, Phys. Rev. C **67** (2003) 045203.
36. R. C. Carrasco, E. Oset and L. L. Salcedo, Nucl. Phys. A **541** (1992) 585.
37. D. Cabrera, L. Roca, E. Oset, H. Toki and M. J. Vicente Vacas, Nucl. Phys. A **733** (2004) 130.
38. M. H. Wood *et al.* [CLAS Collaboration], Phys. Rev. Lett. **105** (2010) 112301 [arXiv:1006.3361 [nucl-ex]].
39. A. Polyanskiy, M. Hartmann, Y. .T. Kiselev, E. Y. .Paryev, M. Buscher, D. Chiladze, S. Dymov and A. Dzyuba *et al.*, Phys. Lett. B **695** (2011) 74 [arXiv:1008.0232 [nucl-ex]].